

AD-A167 070

PHOTOLUMINESCENCE STUDY OF SILICON AND OXYGEN IMPLANTED  
GALLIUM ARSENIDES(U) AIR FORCE INST OF TECH  
WRIGHT-PATTERSON AFB OH SCHOOL OF ENGINEERING K KEEFER

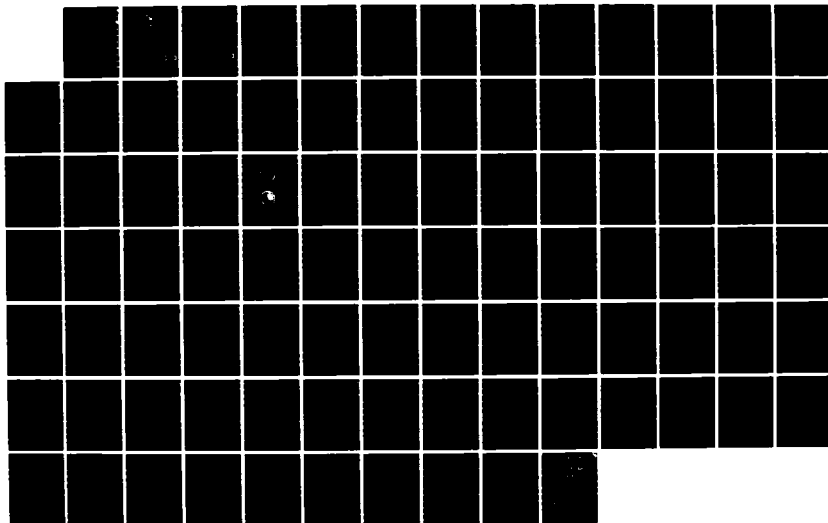
1/1

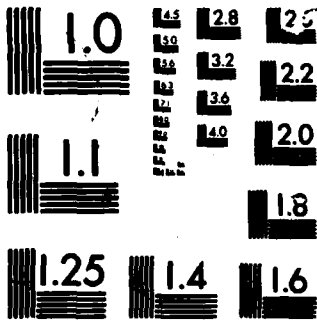
UNCLASSIFIED

DEC 85 AFIT/GEP/85D-8

F/G 20/12

NL





MICROCOPY

CHART

AD-A167 070



PHOTOLUMINESCENCE STUDY OF SILICON  
AND OXYGEN IMPLANTED GALLIUM ARSENIDE

THESIS

Kevin Keefer  
Captain, USAF

AFIT/GER/85D-2

**DISTRIBUTION STATEMENT A**

Approved for public release  
Distribution Unlimited

DTIC  
ELECTE  
MAY 12 1986

DEPARTMENT OF THE AIR FORCE  
AIR UNIVERSITY

**AIR FORCE INSTITUTE OF TECHNOLOGY**

Wright-Patterson Air Force Base, Ohio

86 5 12 034

DTIC FILE COPY

AFIT/GEP/85D-8

PHOTOLUMINESCENCE STUDY OF SILICON  
AND OXYGEN IMPLANTED GALLIUM ARSENIDE

THESIS

Kevin Keefer  
Captain, USAF

AFIT/GEP/85D-8

DTIC  
ELECTE  
MAY 12 1986  
S B D

Approved for public release; distribution unlimited

AFIT/GEP/85D-8

PHOTOLUMINESCENCE STUDY OF SILICON AND OXYGEN  
IMPLANTED GALLIUM ARSENIDE

THESIS

Presented to the Faculty of the School of Engineering  
of the Air Force Institute of Technology  
Air University

In Partial Fulfillment of the  
Requirements for the Degree of  
Master of Science in Engineering Physics

Kevin Keefer, B.S., M.S.

Captain, USAF

December 1985

Approved for public release; distribution unlimited

### Acknowledgements

This thesis was completed with the support and encouragement of many people. I would like to thank my advisors, Dr. R. L. Hengehold and Dr. Y. K. Yeo, for their suggestions and assistance in particular problem areas; thanks also to Jeff Cavins, Jamie Varni, Dave Elsaesser and Marvin Carlson for their development of computer software and general technical assistance. Appreciation also goes to Jim Ehret and Charles Geesner for their assistance in sample preparation. I also want to thank God for bringing these and others to my assistance.

Kevin J. Keefer

(This thesis was typed by Mrs. Allene Mikrut)



Accession For	
NTIS GRAM	<input checked="checked" type="checkbox"/>
DTIC TAB	<input type="checkbox"/>
Unannounced	<input type="checkbox"/>
Justification	
By _____	
Distribution/	
Availability Codes	
Dist	Avail and/or Special
A-1	

## Table of Contents

	Page
Acknowledgements .....	ii
List of Figures .....	v
List of Tables .....	vii
Abstract .....	viii
I. Introduction .....	1
II. Theory and Previous Work .....	7
A. Photoluminescence .....	7
1. Energy States in Semiconductors .....	7
2. Crystal Excitation Absorption & Emission .....	10
3. Radiative Transitions .....	13
3a. Exciton Recombination .....	13
3b. Band-Impurity Transitions .....	16
3c. Donor-Acceptor Pair Transitions ..	17
3d. Phonon Assisted Transitions .....	18
3e. Photoluminescence Spectrum of GaAs ..	18
3f. Photoluminescence of Silicon Implanted GaAs .....	21
3g. Oxygen Associated Peaks in GaAs ..	22
B. Electrical Measurements .....	23
1. Capacitance-Voltage (C-V) Profiling ....	24
2. Hall Measurements .....	25
3. Ion Implantation.....	28
III. Description of Experiment .....	32
A. Sample Preparation .....	32
B. Photoluminescence Measurements-Systems and Procedures .....	40
1. Excitation Source and Optical Detection System .....	40
2. Sample Environment .....	45
C. Electrical Measurements - Systems and Procedures .....	48
1. C-V Profiling .....	48
2. Hall Measurements .....	49
IV. Results and Discussion .....	51
A. Characterization of Control Samples .....	51
1. LEC GaAs .....	52
1a. C-V Measurements .....	52

1b. Luminescence Measurements .....	52
2. Silicon Implanted LEC GaAs.....	55
2a. C-V and Electrical Measurements ...	55
2b. Luminescence Measurements .....	56
3. Oxygen Implanted LEC GaAs .....	59
3a. Luminescence Measurements .....	59
B. Characterization of Silicon and Oxygen ....	63
1. Electrical Measurements .....	63
2. Luminescence Measurements .....	64
V. Conclusions and Recommendations .....	71
A. Conclusions .....	72
B. Recommendations .....	72
Bibliography .....	74
Vita .....	78



## List of Figures

Figure	Page
1. Sheet resistivity versus annealing temperature for Si-implanted GaAs samples bombarded with oxygen .....	5
2. Donor/Acceptor states located within the band-gap	9
3. Fundamental radiative transitions .....	14
4. One dimensional distribution maps of 1.49 eV PL intensities for (a) unannealed and (b) annealed case .....	20
5. van der Pauw Configuration .....	27
6. Implanted ion range distribution .....	29
7. Ratio of peak penetration range $\langle X \rangle_R$ , to damage depth, $\langle X \rangle_D$ , as a function of mass ratio, $M_2/M_1$ .....	30
8. An extrapolated C-V profile used in the determination of a corrected $N_S$ .....	35
9. Ion Implantation Accelerator .....	36
10. Plasma-enhanced deposition system reactor chamber with large shower ring (9:14) .....	37
11. Luminescence measurements system diagram .....	41
12. RCA C31034 spectral response characteristics ...	44
13. Cryogenic Evacuation System .....	46
14. Geometry of double column contacts .....	49
15. Block diagram of automated Hall-effect/Sheet-resistivity measurement system (9:17) .....	50
16. PL of LEC GaAs at 5°K using 4880 Å line. Source intensity: 10 W/cm <sup>2</sup> .....	53
17. Typical C-V profile for Si-implanted GaAs at $\phi = 6E12$ and $E = 100$ keV .....	55
18. PL of Si-implanted GaAs at 5°K using 4880 Å line. Source intensity: 20 W/cm <sup>2</sup> .....	57

19.	PL of Si-implanted GaAs at different sample temperatures using 4800 Å line. Source intensity: 20 W/cm <sup>2</sup> .....	58
20.	Spectra of Si-implanted GaAs at 5.5°K using 3500 Å line. Source intensity: 5.5 W/cm <sup>2</sup> .....	60
21.	PL of O-implanted GaAs at 5.5°K using 3500 Å line. Source intensity: 5.5 W/cm <sup>2</sup> .....	62
22.	PL etch spectra of O-implanted GaAs:Si at 5-8°K using 3500 Å line. Source intensity: 5.5 W/cm <sup>2</sup> . O dose: 1.5 x 10 <sup>12</sup> cm <sup>2</sup> , E = 65 keV. T <sub>A</sub> = 400° C for 2 hrs. ....	65
23.	Ratio of free-to-bound to donor-acceptor pair recombination intensities vs. depth .....	67
24.	Q-band observed in (a) GaAs:Si layers (26) and (b) GaAs:Si+O layers .....	68
25.	PL etch spectra of O-implanted GaAs:Si at 5-8°K using 3500 Å line. Source intensity: 5.5 W/cm <sup>2</sup> . O dose: 3 X 10 <sup>12</sup> cm <sup>2</sup> , E = 65 keV. T <sub>A</sub> = 900° C for 15 min. ....	70

List of Tables

Table		Page
I	Penetration Depths ( $F(x) = .37 F(0)$ ) in GaAs at 4.2°K .....	12
II	Anneal Temperature and Duration .....	39
III	Surface Electrical Measurements for Silicon and Oxygen Implanted GaAs .....	64

Abstract

10 to the 12th power  
10 to the 12th power / sq cm

The low temperature photoluminescence properties of Si-, 0- or (Si+0)- implanted GaAs have been analyzed. Liquid Encapsulated Czochralski (LEC) grown GaAs was implanted with 100 keV silicon ions at a dose of  $6 \times 10^{12} \text{ cm}^{-2}$  and/or 65 keV oxygen ions at a dose of  $1.5 \times 10^{12}$  or  $3 \times 10^{12} \text{ cm}^{-2}$ . The oxygen ion energy was chosen so that its projected range coincided with that of the silicon ion. The Si-implanted layers were annealed at  $850^\circ\text{C}$  for 15 minutes. The 0- and (Si+0)- implanted samples were annealed at  $400^\circ\text{C}$  for two hours or  $900^\circ\text{C}$  for 15 minutes.

Electrical measurements indicated that GaAs:Si+0 layers annealed at  $400^\circ\text{C}$  had resistivities four orders of magnitude larger than the Si-implanted layers. In contrast, the resistivity of the GaAs:Si+0 layers had increased by only a factor of one and a half when annealed at  $900^\circ\text{C}$ .

By comparing spectral features of the differently prepared samples as a function of sample temperature as well as depth within the sample, it was found that there was some correlation between the electrical and optical properties of these layers. The free-to-bound transition ( $e, \text{Si}_{\text{As}}$ ) in the GaAs:Si layers was quenched in the  $400^\circ\text{C}$  annealed GaAs:Si+0 layers, which in turn exhibited relatively high resistivity. However, this particular

17005  
transition was found in the relatively low resistivity GaAs:Si+O layers annealed at 900°C. It is proposed that the implanted oxygen created intermediate levels in the high resistivity samples. The formation of these levels in the low resistivity samples was inhibited, as oxygen appeared to assist rather in the creation of Q-band related complexes that had been normally found in GaAs:Si layers which were capped and annealed.

PHOTOLUMINESCENCE STUDY OF SILICON AND OXYGEN  
IMPLANTED GALLIUM ARSENIDE

I. Introduction

The demand for very high speed digital devices and higher microwave frequency communication systems has been and continues to be strong. Tough requirements in areas such as target acquisition, guidance and control, and electronic countermeasures necessitate improved design and further characterization of semiconductor devices. These requirements are driven by the ever present need to perform the Air Force mission properly.

Monolithic integrated circuit technology relied heavily upon silicon and germanium substrate materials for many years. The advent of a new and better substrate material, gallium arsenide (GaAs) did not change this situation as it could not be utilized until recent improvements in fabrication techniques took place. The properties of GaAs which weigh decisively in its favor for signal processing devices, microwave communication, and radar components are twofold. First, it has two to four times the electron mobility of its counterparts, silicon and germanium and secondly, it has an intrinsic resistance from one thousand to ten million that of silicon and germanium, respectively. The latter characteristic, however, diminishes the

probability of device coupling amongst components of the integrated circuit (1).

Indeed, device isolation has especially become a critical parameter with the relentless miniaturization of the integrated circuit. Thus, further advancements in device isolation techniques, in conjunction with the introduction of improved substrate material, have been both necessary and very beneficial. Many of the isolation methods developed for silicon and germanium substrates were unsuccessful when applied to GaAs. Even mesa etching, a well known isolation technique for silicon and germanium, has been found to be unsatisfactory for the stringent isolation requirements of today's planar device technology. Today, however, many shortfalls using the former techniques, such as nonuniformity across the isolated region and device undercutting, have been overcome with the use of ion implantation.

Foyt, et. al (2:209) first investigated the use of ion implantation as an effective means of device isolation. Prior to that, the semi-insulating layers formed by ion bombardment were considered only in terms of their detrimental effect upon device operation. It is clear that implanting very energetic particles, ions in this instance, will disrupt the relatively ordered nature of a crystalline substance such as GaAs. Gossick (3) demonstrated, via electrostatics and the electrical character of neutron

irradiated germanium and silicon, that the resultant disordered regions act to trap or compensate free carriers. Proton bombardment has been used most extensively because of its large penetration depth, a favorable characteristic for device fabrication (4:14). Implanted layers, however, need to be annealed and the induced semi-insulating properties of such implanted layers have been observed to disappear for annealing temperatures in excess of 350°C (5:621). This thermal instability is not desirable for device fabrication and operation.

An alternative implant species, currently receiving much attention, is oxygen. Although range of penetration of oxygen ions is smaller than that of protons, oxygen ion implantation offers the prospect of good thermal stability. Oxygen-implanted layers, in both n- and p- type GaAs, have remained semi-insulating subsequent to heat treatments as high as 860°C (5, 6). It has been suggested that two different compensating mechanisms are likely in the case of oxygen implantation. The first, of course, is the previously mentioned defect induced compensation. The second is a chemical, doping-induced effect which has been proposed to account for compensation after defects associated with damage have been removed by annealing. In this case, oxygen appears to act as a double electron trap (7:2533). Prior to recent investigations supporting the latter mechanism, Woods and Ainslie (8) had discovered



evidence for the hypothesis of a double electron trap when studying means for altering the electrical properties of GaAs during crystal growth. In this study, GaAs, exposed to high over-pressures of oxygen during growth by the horizontal Bridgeman technique, exhibited semi-insulating characteristics.

A study, stimulated by the above findings and sponsored by the Air Force Avionics Laboratory (9), has been made of the electrical properties of both silicon and oxygen implanted GaAs. Many previous studies of the semi-insulating effect of oxygen implantation had employed epitaxially grown, uniformly doped, GaAs. In addition, oxygen had been implanted at energies in excess of 200 keV with subsequent high temperature anneal. The purpose of the Avionics Lab study was to investigate via electrical measurements, a larger range of anneal temperatures using various oxygen implant doses into ion-implanted, rather than uniformly doped, GaAs. The substrate used was Liquid Encapsulated Czochralski (LEC) grown GaAs. The isolation technique's thermal stability and adaptability to varying applications could be explored. The following rather interesting results were obtained. The sheet resistivity was found to increase with anneal temperatures up to about 400° C. As shown in Fig. 1, the resistivity had increased by an order of seven, after annealing at 400° C, over that of silicon implanted GaAs. This result is in contrast to that

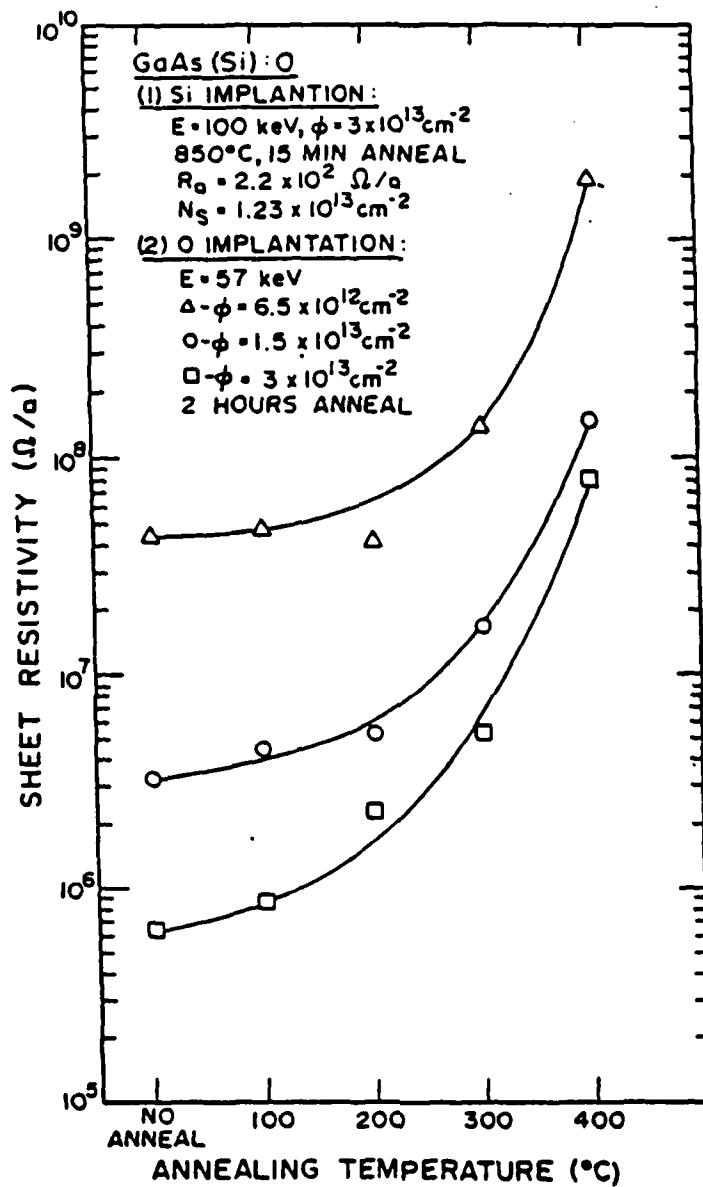


Fig. 1 Sheet resistivity versus annealing temperature for Si-implanted GaAs samples bombarded with oxygen (9:320).

of proton bombardment. In addition, high temperature anneal (500-900°C), subsequent to sequential silicon and oxygen implants, produced n-type conductive layers instead of the high resistivity layers found previously (5, 6). In fact, after a 900°C anneal, the sheet resistivity had increased only by a factor of two over that found for the silicon implanted substrate (10).

This thesis makes use of the technique of photoluminescence to optically investigate silicon and oxygen implanted GaAs layers. The goal was to correlate this information with the electrical data obtained in the Avionics Lab study. To achieve this, the Si-implanted GaAs samples were bombarded with oxygen ions, annealed at temperatures of 400 and 900°C, and then optically examined.

## II. Theory and Previous Work

### A. Photoluminescence

Photoluminescence is an experimental method involving the emission of radiation, which is used to investigate physical processes within semiconductors. As with all spectroscopic techniques, a great deal can be learned about a material's properties from the measured energy transitions. The following sections describe the energy band structure of, and resulting radiative transitions within, semiconductors. Reference will be made to specific transitions previously observed in LEC grown GaAs and GaAs doped with silicon and/or oxygen.

1. Energy States in Semiconductors. A semiconductor has an energy band structure characterized by regions of allowed electronic states, which are referred to as the conduction and valence bands. These are separated by a region of forbidden states called the band gap. McKelvey (11:Ch.8) presents a derivation of these bands in terms of either the tight-binding or nearly free-electron approximation. The use of one over the other depends upon the particular material. In practice, other approximation techniques such as OPW and pseudopotentials are applied to band structure calculations. GaAs is found to have spherically symmetric, parabolic bands near the bottom of the conduction band and top of the valence band

and is a direct-gap semiconductor (12:235). The band gap or energy gap in GaAs has a value of 1.52 eV at 0°K. For an intrinsic semiconductor, the population of holes and electrons within the forbidden region is zero. However, charge carriers in the valence band, upon absorption or emission of energy greater than or equal to the band gap, are able to transit this forbidden region. Thus, one may alter the electrical properties of an intrinsic semiconductor via applied heat, voltage or photons. Almost invariably, though, one must resort to adding impurities to the crystal to achieve essential, well controlled, electrical characteristics for a particular application.

An extrinsic semiconductor, one in which impurity atoms exist within or have been added to the crystal, present a slightly more intricate energy structure. An impurity introduced substitutionally, replacing constituent crystal atoms, is classed either as an acceptor or donor. This depends on whether it accepts an electron from the crystal, creating a free hole in the valence band or donates a free electron to the conduction band of the crystal. The acceptor or donor gives rise to additional states located within the band gap due to the potential energy of the impurity - electron interaction. These states are illustrated in Fig. 2. In fact, this can be conceptualized using the hydrogen-like approximation for both donor and acceptor centers. Thus, the electron or hole ionization

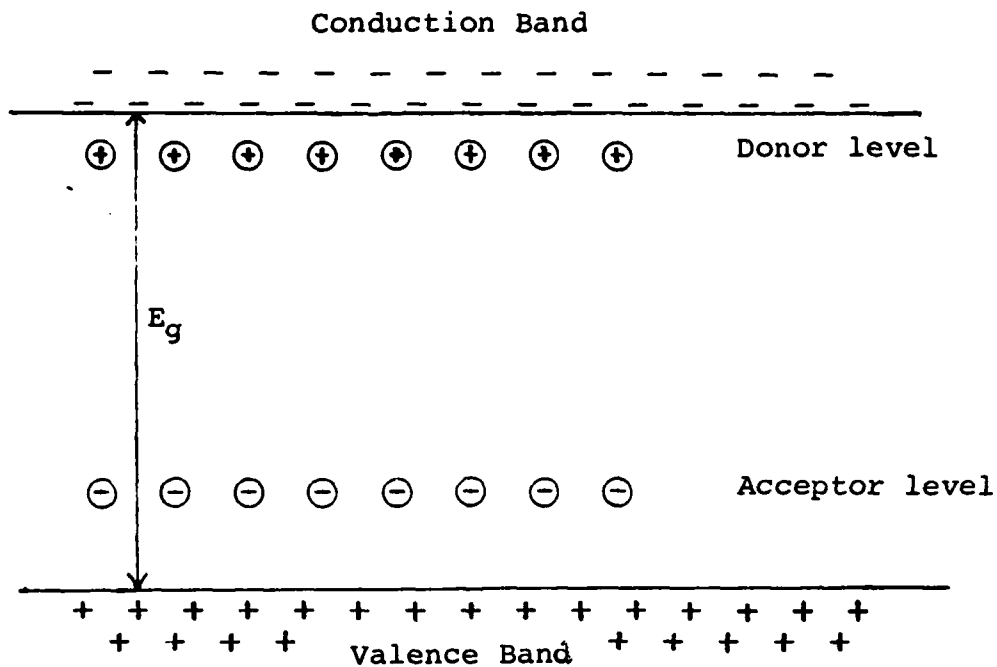


Fig. 2 Donor/Acceptor states located within the band-gap.

energies,  $E_i$ , for various impurities can be determined via the following equation:

$$E_i = (e^4 m^* / 2 \kappa^2 \hbar^2) \quad (1)$$

where  $e$  is the electronic charge,  $m^*$  is the electron or hole effective mass,  $\kappa$  is the dielectric constant of the solid and  $\hbar$  is Planck's constant. This approximation was shown to be valid for many impurities in semiconductors and accurate to within 10% (13:124). Such impurities are termed

simple centers. For example, in GaAs, the donor ionization energy is 5.2 meV and that of the acceptor is 34 meV (14:347). The impurity level itself will actually broaden into a continuous band of states as the impurity concentration increases. This results from the overlap of electron wave functions and has been observed at concentrations as low as  $10^{16} \text{ cm}^{-3}$  (15:9). This broadened level eventually fuses with the conduction or valence band, whichever is closest.

Some other impurities and defects introduced into, or inherently found in, the lattice are classified as complex centers. Such impurities may lodge themselves between constituent atoms and are known as interstitial impurities. Anti-site defects, such as a gallium on an arsenic site in a GaAs crystal, and lattice vacancies are additional examples of complex centers. Normally, these centers create deep, broad energy levels within the band gap which are not predicted by the hydrogenic approximation (14:359).

2. Crystal Excitation, Absorption and Emission. The technique of photoluminescence relies on irradiating the semiconductor with photons. The semiconductor subsequently emits radiation in excess of the thermal equilibrium blackbody radiation. Photoluminescence can be separated into three processes. First, the photons are absorbed and electron-hole pairs are created. Second,

the electron-hole pairs eventually recombine, but not necessarily in the near-surface where they are generated. This is due to the fact that the photo-excited excess carriers have an inhomogeneous spatial distribution within the sample. Therefore, these carriers will have a tendency to diffuse into the sample before recombining, in their struggle to regain a uniform distribution (16:220). The subsequent and third stage of photoluminescence involves the internal emission of photons, resulting from radiative alone or a combination of radiative and non-radiative transitions. These photons escape the sample if not otherwise absorbed or reflected in the crystal. The absorption coefficient for such photons depends on their energy, i.e. those with energy below the band gap energy have a smaller absorption probability.

Before proceeding into a discussion of the potential radiative transitions within semiconductors, the following should be noted concerning the excitation source in photoluminescence. The excitation photon should have an energy greater than the band gap energy in order to increase the probability of absorption, and thus enhance luminescence intensity. In addition, the photon energy, and therefore wavelength, determines the excitation depth. The excitation photon flux,  $F$ , decreases exponentially with depth of penetration according to the following equation (15:88)



$$F(x) = F(0)\exp(-4\pi kx/\lambda) \quad (2)$$

where  $F(x)$  is the photon flux at a depth  $x$  from the surface,  $F(0)$  is that incident on the surface,  $k$  is the extinction coefficient of the solid and  $\lambda$  the wavelength. The approximate photon penetration depths for wavelengths of concern in this investigation are listed in Table I. Although extrapolated from data collected at temperatures other than 4.2°K (12:519,522), the extinction coefficients shown for GaAs are reasonable based on the following assumptions. First, the absorption coefficient, which is proportional to the extinction coefficient, varies only slightly with wavelength at these high photon energies. Secondly, the shift in the absorption edge of GaAs with temperature is very small. Thus, an extinction coefficient at 4.2°K is assumed to be approximately that at 300°K.

Table I  
Penetration Depths ( $F(x) = .37 F(0)$ ) in GaAs at 4.2°K

Wavelength (Å)	Extinction Coeff.	Penetration Depth (Å)
3500	1.95*	145
4880	.375**	1035

\* Estimated From 300°K Data

\*\* Estimated From 21°K Data

The longer wavelengths provide integrated luminescence from a greater cross section of the sample. This information was valuable before etching the samples for layered luminescence.

3. Radiative Transitions. Radiative transitions result when an electron, in an excited state under non-equilibrium conditions, falls to an empty lower energy state. These states include all those mentioned previously, i.e. those of the conduction and valence band, and intermediate states located within the band gap due to impurities and crystal defects (16:194-5). Fundamental transitions observed in this study will be discussed below. Those included are exciton, band -impurity, donor-acceptor pair, and phonon-assisted recombinations. These are depicted in Fig. 3.

3a. Exciton Recombination. Excitons are classified as either free or bound. A free electron and hole may move throughout the crystal as an attached pair -- the electron orbiting about the hole due to the coulomb interaction. This pair is referred to as a free exciton. It occurs most readily in relatively pure samples and at low temperatures. A free exciton may become trapped on a neutral or ionized impurity resulting in a bound exciton orbiting about the impurity. In either case, the free or bound exciton is normally approximated by a hydrogen-like system.

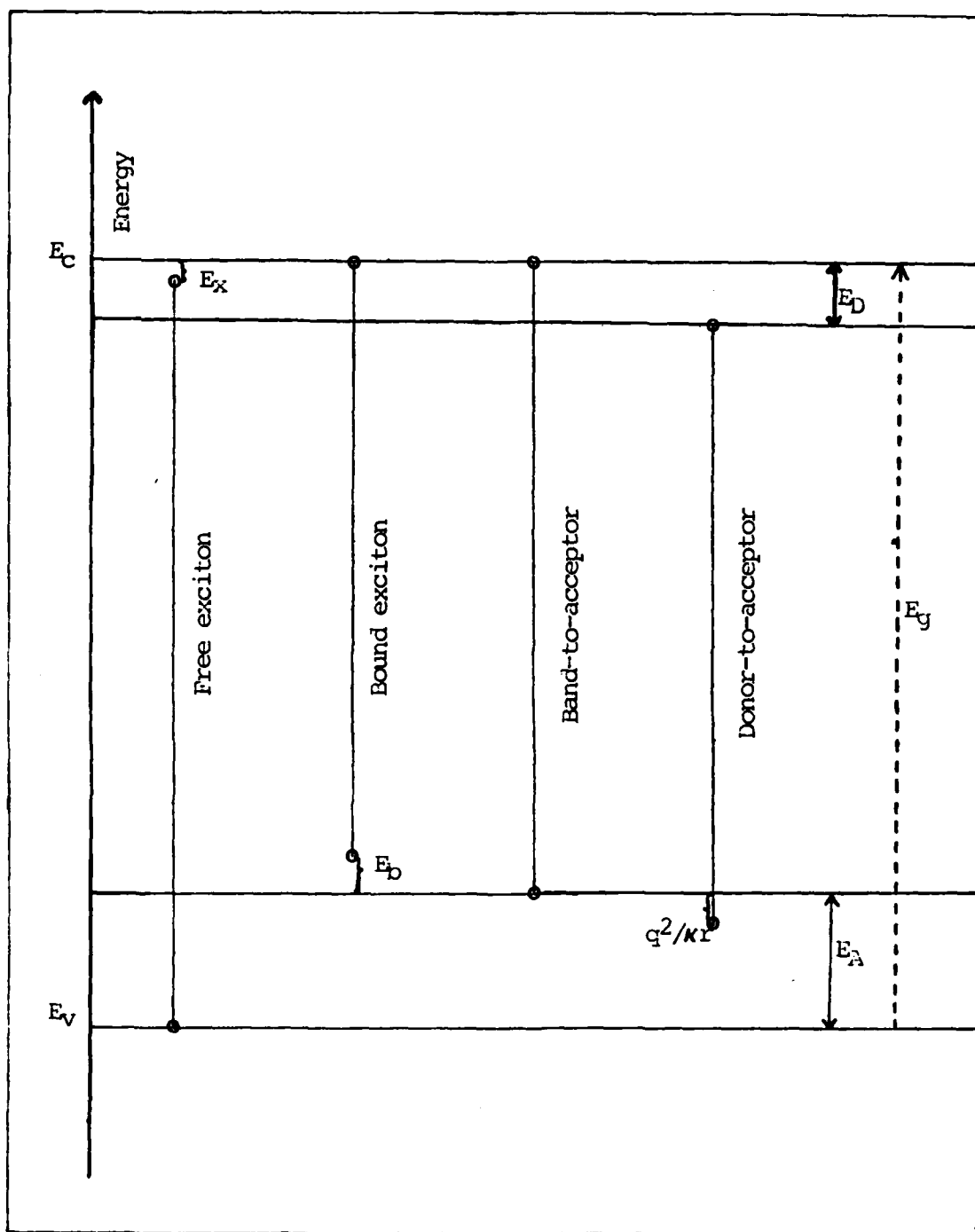


Fig. 3 Fundamental radiative transitions.

A free exciton, using the hydrogenic model, has an approximate ionization energy given by

$$E_x = (m_r^* e^4 / 2 \hbar^2 \kappa^2 n^2) \quad (3)$$

where  $m_r^*$  is the reduced effective mass of the free electron-hole pair and  $n$  is an integer referring to the various exciton states (15:12). For GaAs,  $E_x$  is 4.4 meV (17:995), which compares to an experimentally determined value of 4.2 meV (18:761). Therefore, when an exciton recombines, the emission energy will be simply

$$\hbar\omega = E_g - E_x \quad (4)$$

In III-V compounds, such as GaAs, all of the exciton states, except  $n=1$ , have a recombination energy within 1 meV of the band gap energy and therefore are not easily distinguished (16:284). However, these can be differentiated, using a magnetic field, by capitalizing on the Zeeman effect (18:761-767). The ground-state free exciton recombination has given rise to a narrow peak at 1.5153 eV (18:763) in the GaAs photoluminescence spectrum. The free exciton can be thermally ionized. Therefore, this peak's intensity would be expected to decrease with an increase in temperature and become negligible at temperatures much larger than 50°K.

The recombination energy of a bound exciton can be approximated with a slight modification of Eq (4) such that

$$\hbar\omega = E_g - E_x - E_b \quad (5)$$

where  $E_b$  refers to the energy binding the free exciton to the impurity. The impurity can take many forms including both ionized and neutral donors and acceptors.  $E_b$  has been determined to be a function of the electron-hole effective mass ratio of any particular crystal (19, 20). It is normally given in terms of the isolated acceptor or donor ionization energy. The bound exciton emissions differ from those of the free exciton in that they are much narrower (15:116). Their intensity can also be expected to decrease with increased temperature, as the complex thermally dissociates into a free exciton and the impurity.

3b. Band-Impurity Transitions. Band-impurity or free-to-bound (FB) transitions include the transition of an electron from a donor to the valence band or that from the conduction band to an acceptor. Most generally, the recombination emits a photon with energy given by

$$\hbar\omega = E_g - E_i \quad (6)$$

where  $E_i$  refers to the ionization energy of the impurity -- acceptor or donor -- as given by Eq (1). As discussed

earlier, the impurity levels broaden with increased impurity concentrations. Thus, one would expect the emission peak, due to these transitions, to do likewise. If the impurity concentration becomes large enough to form a continuum of states fused with the conduction or valence band, band-impurity transitions become much less probable and their associated peaks are hard to identify (15:133-134).

3c. Donor-Acceptor Pair Transitions. It is entirely possible that a donor shares an electron with an acceptor in the crystal. This pair's individual ionization energies are thus modified according to the familiar coulombic potential due to free charge. Therefore, if the electron subsequently recombines with the hole associated with the acceptor, the energy emitted will be given by

$$\hbar\omega = E_g - E_A - E_D + (q^2/\kappa r) \quad (7)$$

where  $E_A$  and  $E_D$  refer to the ionization energies of the acceptor and donor, respectively, (see Eq (1)), and  $r$  of the last term represents the distance separating the acceptor and donor. Assuming substitutional impurities, the coulomb correction term will take on distinct values due to the periodic spacing of lattice sites within the crystal. In fact, a series of sharp luminescence lines, corresponding to individual pairs, can be resolved. These

sharp pair luminescence lines are in close proximity to a broad peak. This broad peak is made up of many overlapping peaks resulting from distant donor-acceptor pair recombinations. In the absence of sharp pair lines, donor-acceptor transition peaks may be identified by varying the donor concentration in the crystal. One would expect the separation distance,  $r$ , to increase with decreased donor concentration. Therefore, according to Eq (7), the peak should shift to lower energy (15:17-18,143; 14:335-336).

3d. Phonon Assisted Transitions. As mentioned previously, GaAs is a direct gap material. Therefore transitions between states do not require the assistance of phonons to conserve momentum. Nonetheless, radiative energies for transitions involving impurities, may be changed due to phonon coupling. Electrons or holes bound to a substitutional impurity may interact with lattice vibrations, thus detracting from radiative emission energy if recombination occurs. The longitudinal optical (LO) phonon has an associated energy of 36 meV for GaAs. Any number of these quanta may be associated with a transition and thus several lower-energy replicas of the "mother" peak may be observed in the photoluminescence spectrum (14:387-388).

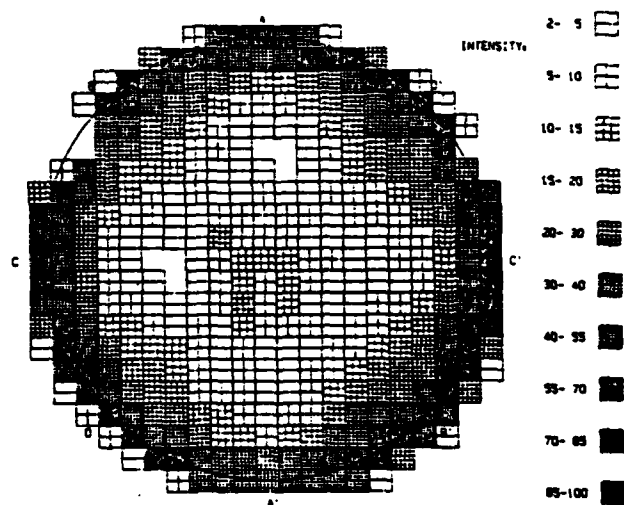
3e. Photoluminescence Spectrum of GaAs. The photoluminescence spectrum of GaAs substrate material

certainly depends upon the method of crystal growth. Each method, and for that matter, the laboratory in which the method is used, introduces certain contaminants or defects which in turn affect the radiative spectrum. The substrate used here was grown by the LEC technique in a graphite crucible. Therefore, it seems appropriate to highlight the expected near-band luminescence of such crystals.

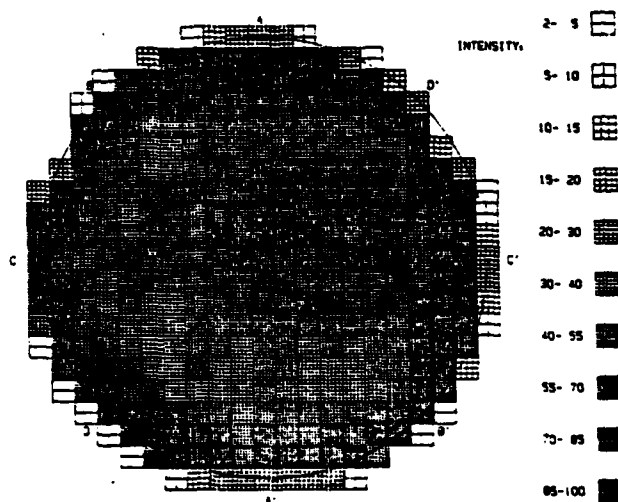
The major line, sometimes referred to as a band, observed in the edge photoluminescence of LEC crystals is that at approximately 1.49 eV. It is made up of an 1.490 eV donor-acceptor ( $D^+, A^-$ ) peak, and an 1.494 eV conduction band-to-acceptor ( $c, A^-$ ) peak (21:582). These transitions arise from a substitutional carbon impurity on an arsenic site (22:864). It is interesting to note that the ambient gas used in the growth process may affect this band's intensity. This band was observed in nitrogen, helium and krypton ambients, but hardly so in an ambient of argon (23:1654). In addition, the severe thermal environment of LEC growth results in high dislocation densities in the substrate. These subsequently lead to radial variations of the intensity of the 1.49 eV line across the wafer substrate (24:L339). Whole-ingot annealing following growth is a suggested remedy. The phenomenon and annealing effects are shown in Fig. 4.

A secondary lower lying peak has been tentatively explained as due to an antisite  $Ga_{As}$  defect acting as a





a.



b.

Fig. 4 One dimensional distribution maps of 1.49 ev PL intensities for (a) unannealed and (b) annealed case (24:L340-L341).

residual acceptor. It is located at approximately 1.44 eV and found in crystals grown from melts of less than 0.47 As mole fraction (25:274).

Finally, one may observe high energy peaks representing both the free exciton and bound exciton transitions. Because the free-exciton line does not result from an impurity-related transition, it can be expected for any crystal, no matter how prepared. The reported energy of 1.512 eV has been associated with an exciton bound to a neutral carbon acceptor recombination (21:582).

3f. Photoluminescence of Silicon Implanted GaAs. Few results have been published for silicon implanted GaAs. In addition, those published have not all been at the low sample temperatures, implant energy, nor dose contemplated in this investigation. Nonetheless, such results are valuable for comparison.

One characteristic, is the existence of a broad low energy band between 1.39 and 1.47 eV. Pomrenke, et. al. (26) observed a broad band at 1.465 eV for an 850°C annealed sample. Their investigation concluded with the postulate that the Q-band, as it was called, was due to three competing complexes, all of which involved silicon in some manner. It was interesting to note that silicon was acting as an acceptor in two out of the three complexes mentioned. Another study, by Voltsit et. al. (27), assigned a broad peak at 1.455 eV to relatively deep donor

centers, possibly implying that silicon was occupying gallium sites. For anneal temperatures greater than 750°C subsequent to implant, this peak's intensity diminished. This result seemed to correlate with those of the Pomrenke study.

3g. Oxygen Associated Peaks in GaAs. Several investigations have associated various peaks in the spectra of as-grown crystals with oxygen. Near-edge peaks will be presented first, followed by those at low energy levels resulting from defects induced by oxygen implantation. Finally, very low energy peaks, i.e. less than .9 eV, that have been observed will be summarized. Defining the oxygen-related centers giving rise to such peaks has been a difficult task. Such information will be provided where available.

Peaks at 1.5138 and 1.489 eV, associated at least tentatively with oxygen and assigned as bound exciton transitions, have been observed (28:29:30). Both peaks were reported for GaAs chemically doped with oxygen, while only the 1.489 eV line was observed in oxygen implanted samples. Other peaks, found in oxygen implanted GaAs, include those at 1.482 and 1.472 eV (29:495). Only one or the other was observed, depending upon the method of crystal growth.

Low energy peaks have arisen more as a result of defects caused by implantation than due to the presence of oxygen

itself. It was noticed by Monemar and Blum (31) that the recovery rate of the decreased photoluminescence intensity, subsequent to implant, was substantially increased for anneal temperatures greater than 450°C. In this temperature range, defects -- gallium and arsenic vacancies -- created by oxygen implantation were able to redistribute to form complexes with nearest-neighbors in the crystal. These complexes acted as important radiative recombination centers resulting in broad, low energy peaks at approximately 1.23 and 1.37 eV. Of course, the exact energy will depend upon the particular complex composition. An additional peak at 1.20 eV has been observed. It is postulated to result from the oxygen occupation of an interstitial site, acting as an acceptor (32,33,34). It is suggested that this acceptor then forms a complex with an ionized donor ( $D^+, O_i$ ) such as silicon (33:426).

The origin of the very low energy peaks is not well understood. Those observed include 0.65, 0.70, 0.76 and 0.82 eV (32,29,35). A model, proposed for these peaks' origin, hypothesizes that a substitutional oxygen ( $O_{As}$ ), acting as an acceptor, forms a complex with an arsenic vacancy ( $V_{As}$ ), i.e.  $O_{As} - V_{As}$  (36:605). The first two peaks are found in both oxygen implanted and doped GaAs.

#### B. Electrical Measurements

The following discussion provides a summary of the theoretical background necessary to understand the

electrical measurements conducted in this investigation. These measurements were meant to be auxiliary to the optical measurements.

1. Capacitance-Voltage (C-V) Profiling. To understand the method of obtaining a carrier profile by applying a voltage to a sample and measuring the resultant capacitance, one can consider the following. Assume a metal is brought into contact with an n-type semiconductor crystal, where the work function of the metal is larger than that associated with the semiconductor. The resulting potential difference at the contact ultimately creates a positive space charge region, or depletion region, which is just an excess of ionized donor atoms. This region is found at the semiconductor surface. If an external voltage is applied across the depletion region, then the width of the region will be changed. An applied reverse bias voltage will increase the width of this depletion region, whereas an applied forward bias will decrease it. This region is thus very similar to a voltage-dependent parallel plate capacitor. The capacitance, therefore, of the space charge region can be written as

$$C = \frac{\epsilon A}{x} \quad (8)$$

where  $\epsilon$  is the permittivity of the material,  $A$  the surface area over which the bias voltage is applied, i.e. the

metal/semiconductor contact area, and  $x$  is the width of the depletion region (37:214). By increasing the reverse bias voltage, the depletion width increases, reducing the barrier capacitance. The number of ions present in the depletion region which result from such an increment of voltage  $dV$  is simply the product of the depletion width,  $dx$ , the area over which the voltage was applied,  $A$ , and the carrier concentration  $N(x)$  at the edge of the depletion region, i.e. between the depleted and non-depleted regions. Heinisch (37:216) derived a formula relating the differential change in capacitance with bias voltage to the carrier concentration at the depletion region's edge:

$$N(x) = 2 \left[ e \epsilon A^2 d \frac{(1/C)}{dV} \right]^{-1} \quad (9)$$

where  $e$  is the electronic charge. From such a relation, profiles of the carrier concentration with depth can be calculated.

2. Hall Measurements. Parameters such as the average sheet resistance,  $\rho_s$ , and sheet carrier concentration,  $N_s$ , for a semiconductor material, can be determined by the standard van der Pauw technique. The technique requires that four contacts be placed on the periphery of a semiconductor surface. The specimen may have any shape but must be uniformly thick. In order to allow for any

shape, van der Pauw showed that it was necessary to measure current and voltages across different pairs of contacts (38). This is illustrated in Fig. 5.

The preceding connections, along with the following relations, enable one to determine  $\rho_s$  and  $N_s$ .  $\rho_s$  can be found following measurements of the resistances  $R_a$  and  $R_b$ .  $R_a$  is due to the voltage difference across points one and two and the current  $I$  of Fig. 5a. Likewise,  $R_b$  is ascertained using the Fig. 5b configuration.  $\rho_s$  is calculated using

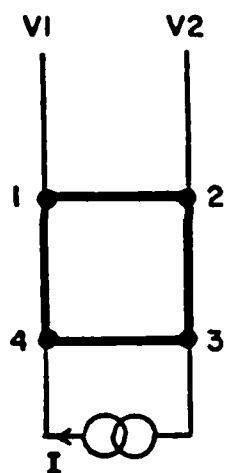
$$\rho_s = (\pi/\ln 2) ((R_a + R_b)/2) f \quad (10)$$

where  $f$  is a geometrical correction factor, dependent on the ratio of  $R_a$  to  $R_b$  (38:6). It is approximately unity for  $R_a/R_b$  of approximately one.  $N_s$  is determined by first finding the sheet-Hall coefficient which is given by

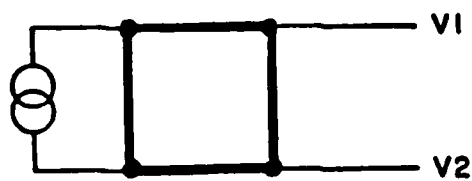
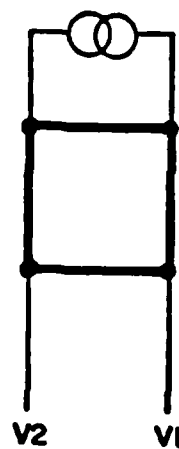
$$R_{HS} = 10^8 (\Delta R / B) \quad (11)$$

where  $B$  is the magnetic field applied normal to the sample and  $\Delta R$  is the change in resistance across points one and two in Fig. 5c due to the applied magnetic field. Having determined  $R_{HS}$ ,  $N_s$  is given by

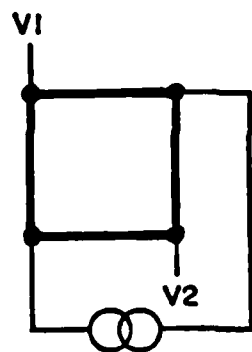
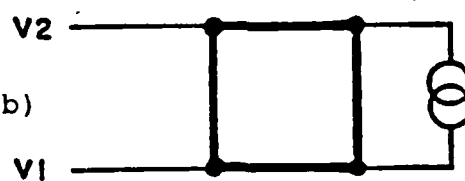
$$N_s = r/eR_{HS} \quad (12)$$



(a)



(b)



(c)

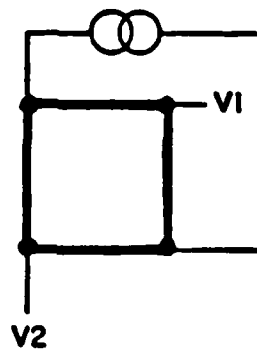


Fig. 5 van der Pauw Configuration.



where  $r$  is the Hall-to-drift mobility ratio which is normally taken to be one (39:3704).

### C. Ion Implantation

Ion implantation involves the introduction of various atomic species into a solid substrate by bombarding the substrate with high energy ions. The technique essentially relies upon the use of an ion source, ion acceleration through a potential, and a mass separating magnet to remove unwanted impurity ions. Advantages to using this technique include low process temperatures, ease of masking and control of ion dose. Depth distribution and damage related to ion implantation will be discussed below.

An important consideration in semiconductor fabrication is the depth distribution of the dopant species. For ion implantation, this profile is a function of the ion's energy and the integrated beam current, which is essentially the ion dose. In most instances, the profile or range distribution is roughly Gaussian in shape and demonstrated in Figure 6. The distribution is characterized by a mean projected range,  $R_p$ , and its standard deviation,  $\sigma_p$ . The theoretical backdrop for predicting these parameters, based on ion mass, energy, and dose, is the Lindhard, Scharff and Schiott (LSS) calculation. This theory models the collisions and interactions experienced by the implanted ion as it moves through the substrate.

GAUSSIAN APPROXIMATION OF IMPURITY CONCENTRATION,  $N(x_p)$ :

$$N(x_p) = \frac{\phi}{\sigma_p \sqrt{2\pi}} \exp\left(-\frac{(x_p - R_p)^2}{2\sigma_p^2}\right), \quad (13)$$

WHERE  $\phi$  IS ION DOSE/CM<sup>2</sup>, AND  $x_p$  IS A MEASURED DISTANCE ALONG THE DIRECTION OF INCIDENT ION BEAM.

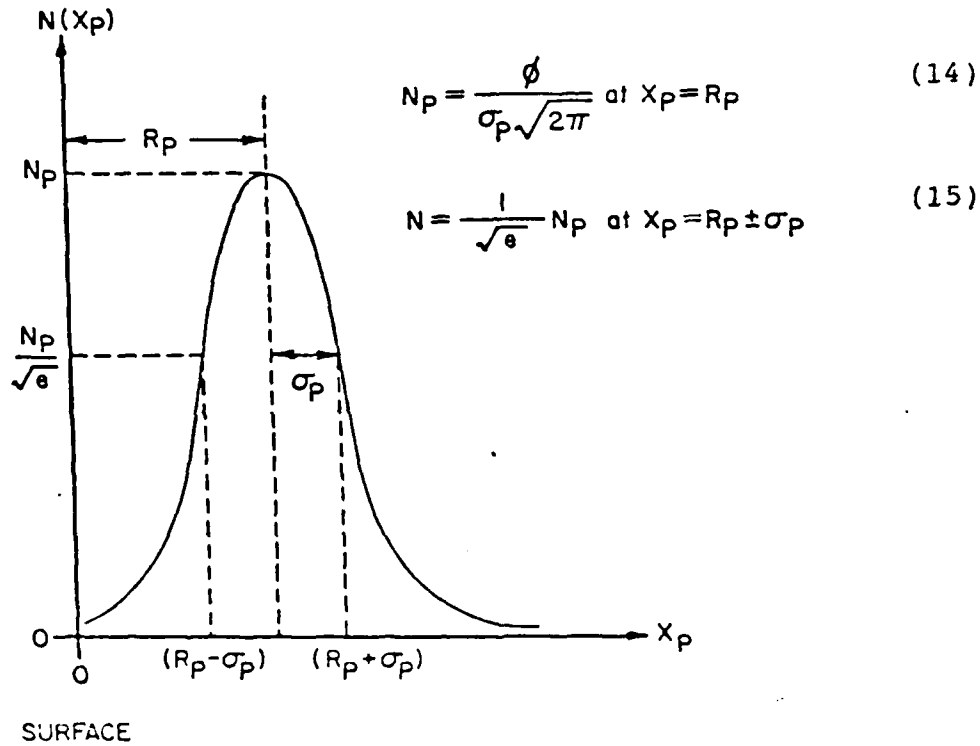
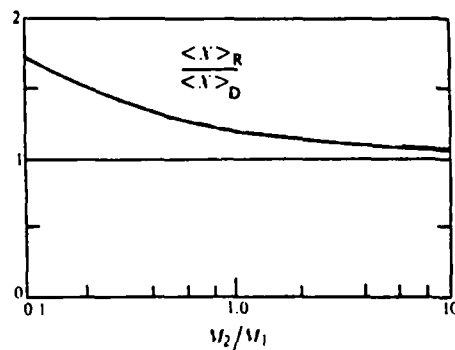


Fig. 6 Implanted ion range distribution.

Implanted ions may become channelled along one of the axes of the single crystal lattice.

If channelling occurs, the implant will lodge itself deeper in the substrate than predicted by LSS theory. This is usually not desired for controlled experimental situations and thus the ions are implanted off-axis.

The disorder produced by the implanted ion, as it pushes through, and comes to rest in, the substrate, is important as it affects both electrical and optical characteristics. The disorder may include crystal vacancies and interstitially located atoms. Experimental and theoretical investigations have been conducted to determine the relative position of the implanted ion distribution and related damage distribution. Fig. 7 shows the result of such a calculation.



$M_2$  = Mass of target atom  
 $M_1$  = Mass of implanted ion

Fig. 7 Ratio of peak penetration range,  $\langle X \rangle_R$ , to damage depth  $\langle X \rangle_D$  as a function of mass ratio,  $M_2/M_1$  (40:134).

Appropriate heat treatment subsequent to implantation has been found to be an effective means of restoring the crystalline order. The appropriate treatment depends on the amount of damage and hence on the ion's energy and dose.

### III. Description of Experiment

This section describes sample preparation, experimental systems, and associated operating procedures.

#### A. Sample Preparation

The substrate material was LEC grown GaAs wafers with  $\langle 100 \rangle$  orientation. The wafers were cut into 6.35 mm by 6.35 mm square pieces. To obtain uniform slices, emphasis was placed on finding and then cutting along the  $\langle 100 \rangle$  axis.

Having partitioned the wafer, the samples were cleaned according to the following procedure:

1). The sample surface was brushed lightly with a swab soaked in diluted basic-H solution. The sample was then rinsed with deionized water. This step was undertaken with care due to possible scratching of the surface.

2). The surface was flushed with the following in the order listed: diluted basic-H solution, deionized water, trichloroethylene, acetone, methanol, and deionized water. This combination insured the removal of grease and other impurities from the surface. It was blown dry with nitrogen gas.

3). Several samples were examined by dark-field microscopy. If residue persisted, the second step was repeated.

Subsequent to cleaning, all samples were free-etched. This step removed any remaining mechanical damage imparted to the surface during crystal fabrication. Ideally, one will be left with a damage-free surface. The etchant consisted of water, hydrogen peroxide and sulfuric acid in

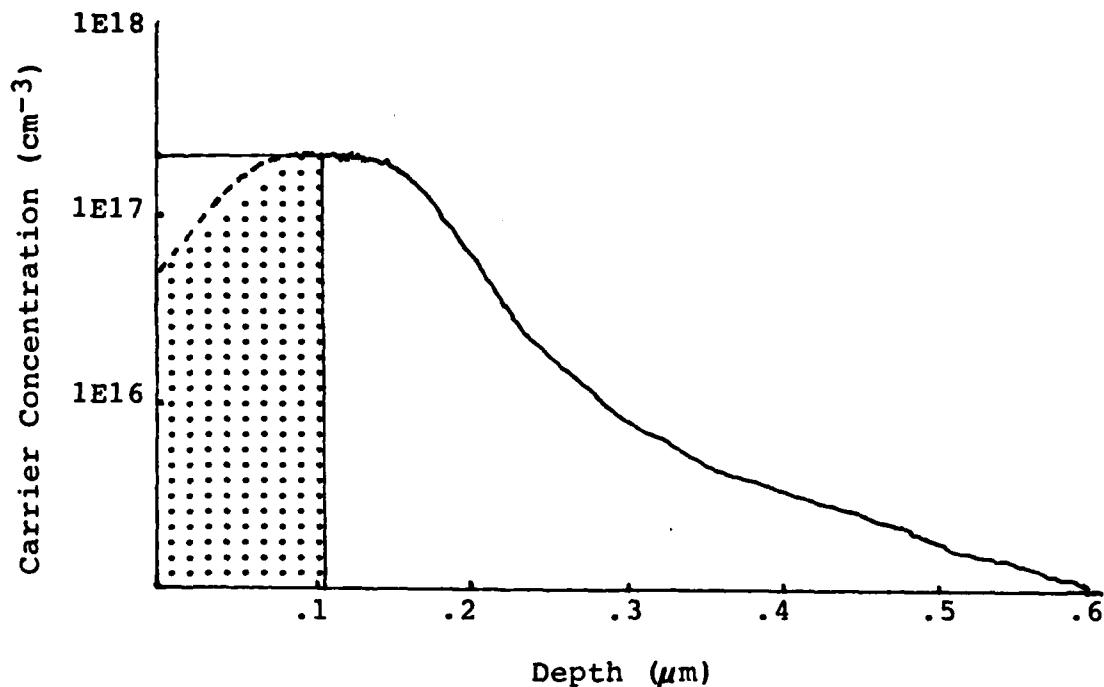
the ratio of 1:1:7. The water and hydrogen peroxide were mixed first. Sulfuric acid was then added, never allowing the mixture's temperature to rise above 30°C. This protected the integrity of the hydrogen peroxide. The samples were etched in a teflon beaker which was constantly agitated to keep bubbles from forming on the sample surface. Such bubbles will lead to a non-uniformly etched surface. The free-etching step was normally accomplished just prior to subsequent sample processing steps to minimize the development of oxides on an otherwise clean surface.

Samples were implanted with silicon and/or oxygen ions at various energies and doses. The silicon implants were made at an energy of 100 keV and dose of  $6 \times 10^{12} \text{cm}^{-2}$ . The low dose was expected to enhance the distinctive features of the photoluminescence data and perhaps aid in its interpretation. The oxygen implant combinations were chosen based upon several inputs. These included Hall measurements and C-V profiles of representative silicon implanted samples, as well as a study which investigated the surface depletion characteristics of silicon implanted GaAs (41). Of particular interest was the derived sheet concentration,  $N_s$ , for the silicon implanted sample. To compensate the electrical activity, oxygen doses were chosen to be either equal to or one-half  $N_s$ . The results reported by Pronko, et. al (9:320) indicated lower

resistivities for oxygen doses in excess of one-half  $N_S$ . The computed  $N_S$ , determined by electrical measurement, was found to be  $2 \times 10^{12} \text{ cm}^{-2}$ . This figure was corrected for the effect of the depletion region. The correction, which was performed by estimating the area under an extrapolated C-V profile for a representative sample, is schematically shown in Fig. 8. This correction was then compared with that from the aforementioned study of depletion effects at a surface-air interface. The final corrected value for  $N_S$  was  $3 \times 10^{12} \text{ cm}^{-2}$ . Thus, oxygen doses of  $1.5 \times 10^{12} \text{ cm}^{-2}$  and  $3 \times 10^{12} \text{ cm}^{-2}$  were the actual implanted doses. The oxygen implant energy was picked so that the projected range for this species approximately matched that of the implanted silicon. This implant energy was determined to be 65 keV using LSS theory.

The implants were accomplished by the Air Force Avionics Laboratory using a Varian/Extrion Model 400-10AR Ion Implanter. A schematic of the machine is shown in Fig. 9. The samples were mounted with their surface normal oriented  $7^\circ$  from the beam current direction to minimize channeling. They were implanted at room temperature.

Subsequent to implantation, it was usually desired to anneal the samples. If this were done at temperatures greater than  $400^\circ\text{C}$ , they were encapsulated first with a dielectric coating. The cap discouraged the outdiffusion of the implanted species as well as surface decomposition of



\*  $N_S$  corrected equals  $N_S$  plus  $\Delta N_S$ , where  $\Delta N_S$  is the area of the shaded region.

Fig. 8 An extrapolated C-V profile used in the determination of a corrected  $N_S$ .

the GaAs since arsenic can dissociate from gallium at a temperature as low as 400°C (9:5).  $\text{Si}_3\text{N}_4$  was used as an encapsulant and the capping process used was plasma-enhanced deposition (PED). Figure 10 depicts the PED system. Before placing the sample in the chamber, it was again cleaned and subjected to a one-minute hydrochloric acid etch to remove any oxides. If this were not



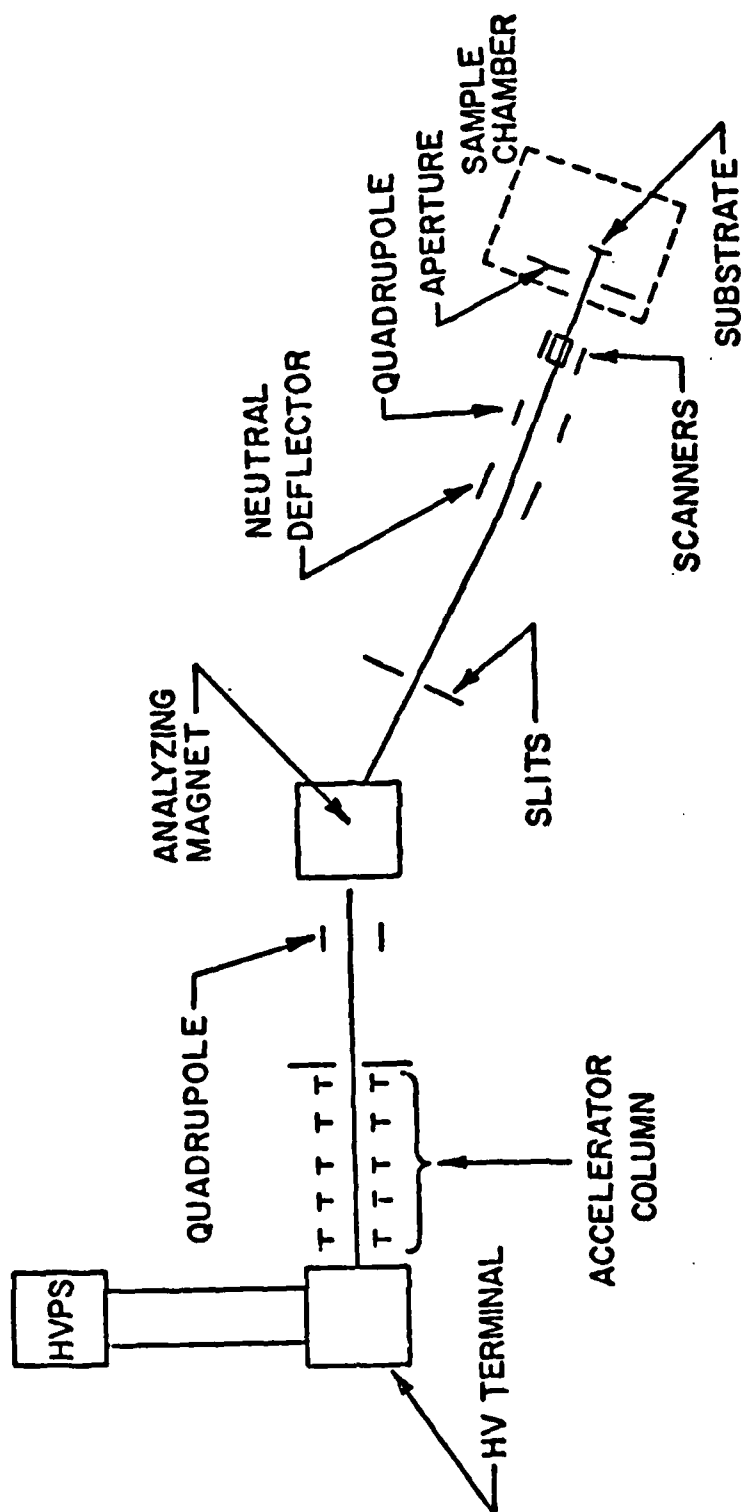


Fig. 9 Ion-Implantation Accelerator

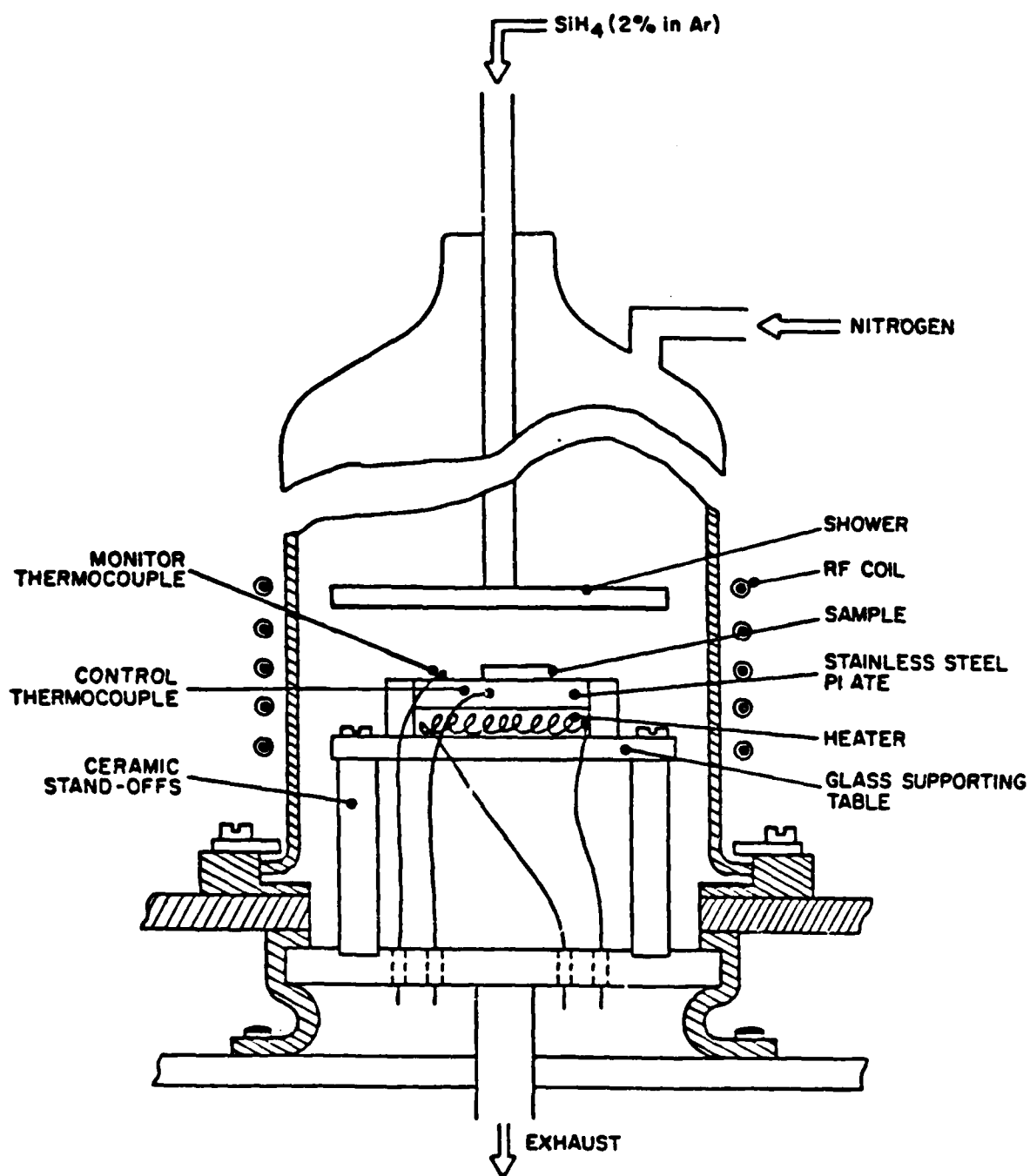


Fig. 10 Plasma-enhanced deposition system reactor chamber with large shower ring (9:14).

accomplished, the cap might not have adhered properly. After placing the sample in the chamber, it was evacuated to  $10^{-6}$  torr and backfilled with nitrogen gas to .45 torr. The sample was then heated to  $400^{\circ}\text{C}$ . Silane ( $\text{SiH}_4$ ), 2% in argon, was then pumped into the chamber while simultaneously initiating a RF plasma within. Decomposition of the  $\text{SiH}_4$  begins immediately. Subsequently,  $\text{Si}_3\text{N}_4$  was deposited onto the sample surface. The desired thickness was  $1000 \text{ \AA}$ . Following encapsulation, an ellipsometer and minicomputer were used to determine the actual thickness of the coating and its index of refraction. Indices which fell below two usually indicate that there may have been an atmospheric leak during the deposition. Those which were greater than 2.06 denoted too rich a silicon mixture. If the cap's index of refraction fell between these ranges, it was of good quality and was expected to provide the desired protection. There were cases where the index of refraction fell in the range of 2.09 through 2.14. The system operator at the Avionics Laboratory, however, believed that these indices were a consequence of excessive damage created in the substrate and were not to be particularly concerned about. The samples that were to be annealed at  $400^{\circ}\text{C}$  were not encapsulated, but extra care was taken to protect against decomposition of the GaAs. This entailed lying the sample face down onto a face-up GaAs substrate during annealing.

Where required, the samples were annealed at the Avionics Laboratory in furnaces with either flowing nitrogen or hydrogen gas. The flowing gases were intended to prevent oxidation at the sample surface. Hydrogen was used at temperatures greater than 600°C. The anneal temperatures and durations are listed in Table II.

Table II  
Anneal Temperature and Duration

Temperature (°C)	Duration (min)
400	120
*850	*15 min
900	15 min

- \* This temperature and duration was used for anneal subsequent to all silicon implants.

After anneal, the caps were removed by soaking in hydrofluoric acid. The cap's blue color was replaced by dark blue, then brown, and finally the metallic color of the GaAs substrate. Three to five minutes additional etch was allowed to insure complete encapsulant removal. If at all possible, caps were left on the sample until just prior to electrical or luminescence measurements.

The last sample preparation step was sample etching in order to carry out the depth resolved luminescence measurements. Black wax was put at the sample's four

corners. Then samples were dipped into a 300 ml solution of  $\text{H}_2\text{SO}_4:\text{H}_2\text{O}_2:\text{H}_2\text{O}$  with a ratio of 1:1:100. The samples were etched at  $0^\circ\text{C}$ . The etching time was determined by the layer thickness to be removed and etch rate, which for this mixture is known to be approximately  $2 \text{ \AA}/\text{sec}$ . After all layered luminescence results were obtained, the black wax was removed. A Sloan Dektak Profilometer was used to measure the step height between the etched surface and that protected by the black wax. This value was divided by the total etch time to provide the average etch rate. This rate was then multiplied by the etch time for each layer removal step to provide the removed layer's thickness.

#### B. Photoluminescence Measurements - Systems and Procedures

The photoluminescence data was gathered using the following procedures and system. The system is depicted in Fig. 11.

1. Excitation Source and Optical Detection System. The primary excitation source was a Spectra Physics Series 2000 Krypton Ion Laser. The desired ultraviolet radiation emanated from a transition between excited states of doubly ionized krypton. An electric discharge was used to excite the krypton atoms which were contained within a plasma tube. To obtain maximum power, proper current settings were required for the plasma tube and circumferential magnet. Because of limited electrical service to the laser power

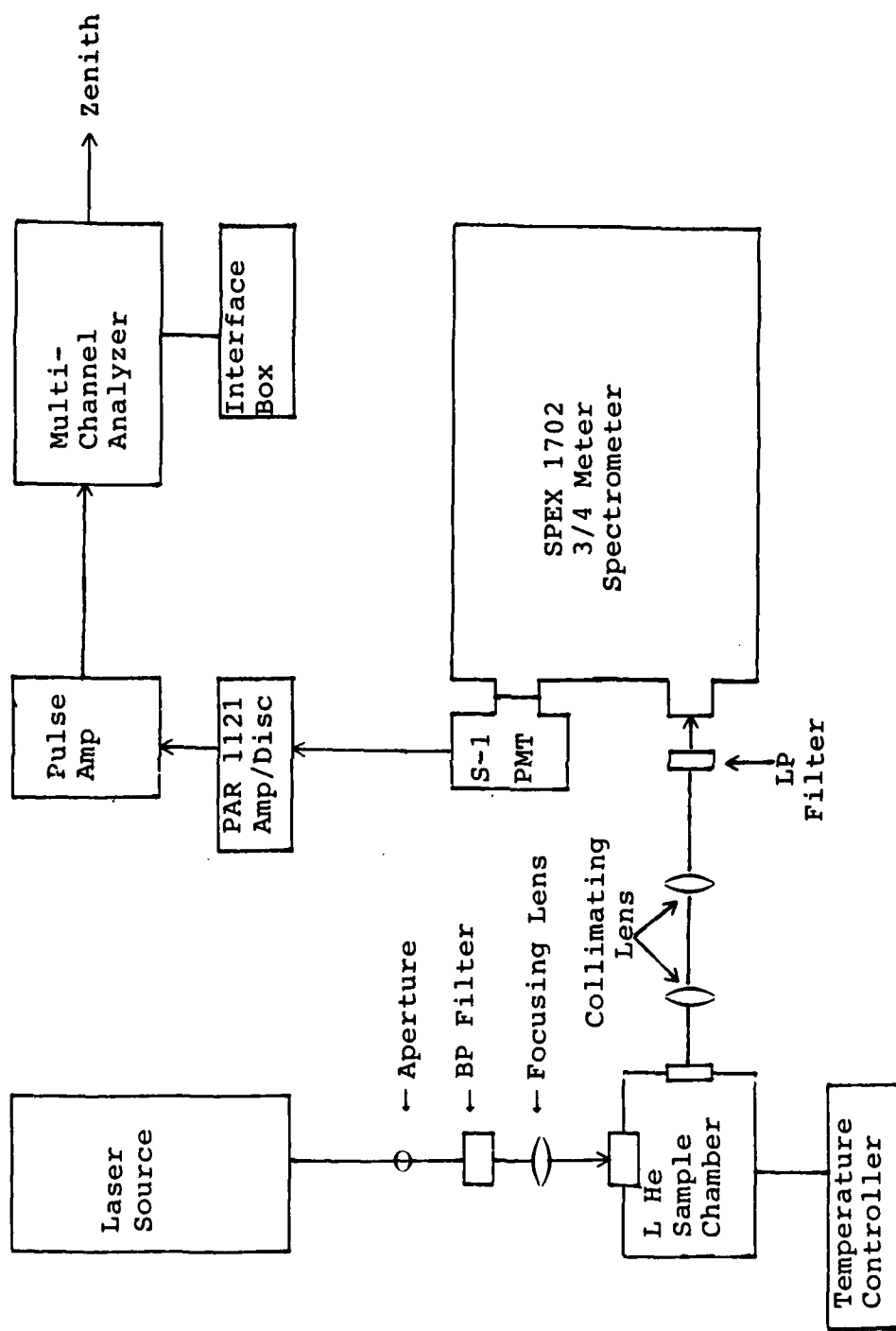


Fig. 11 Luminescence measurements system diagram

supply, the ultraviolet intensity was optimized by first setting the magnet current for approximately 9 amps. Then the remaining current capacity of about 46 amps was applied to the plasma tube. The maximum achieved output power was 70 mW. An infra-red absorbing filter, which was 80% transmissive at  $3500 \text{ \AA}$ , reduced this to approximately 40 mW. To counter defocusing of the output beam by the intermediate optics, which also included a periscopic mirror, a lens ( $f=150\text{mm}$ ) was inserted into the beam prior to its arrival at the sample chamber, thus producing a spot size at the sample of approximately 1 mm. As a result, the maximum power density on the sample was  $6 \text{ W/cm}^2$ . Initial measurements were made using a Spectra-Physics Model 164 argon laser. The output power was 475 mW at  $4880 \text{ \AA}$  with intermediate optics reducing this to 175 mW. Thus, with a spot size on the sample of 1 mm, maximum power densities of  $20 \text{ W/cm}^2$  were produced. When necessary, neutral density filters were used to decrease this.

Several optical devices were used to direct the laser radiation onto the sample, to focus the resulting luminescence onto the spectrometer entrance slit, and to diminish unwanted radiation. Those components preceding the sample chamber have already been mentioned above. The infra-red absorbing filter served to remove undesired krypton gas lines and stray plasma tube emissions. The sample chamber itself had entrance and exit windows made of

quartz. Two f6 lenses were placed between the sample chamber and spectrometer to focus the luminescence onto the spectrometer's entrance slit. Finally, a long pass filter, which was placed directly in front of the entrance slit, eliminated scattered laser radiation and decreased background "noise."

The optical radiation emitted by the sample was dispersed by a Spex 1702, 3/4 meter Czerny-Turner spectrometer. A grating blazed for 5000 Å, with 1200 lines/mm, was used. Thus, the grating's region of usefulness extended from 3400 to 10000 Å (42:57). The spectrometer dispersion was between 10.3 Å/mm and 8.9 Å/mm over the range between 8100 Å and 9900 Å, respectively. Thus, with typical slit widths of 200 and 500 μm, the resolution was better than 1 meV.

The final element of the optical detection system consisted of several electronic components used to collect and record the photon count rate as one scanned across the wavelength spectrum. These included a liquid nitrogen cooled photomultiplier tube (PMT) which consisted of a GaAs photocathode -- RCA type no. C31034. Its response curve is shown in Fig. 12. The output pulses at the anode of the PMT, resulting from photons striking the photocathode, were sent to a Princeton Applied Research Model 1121A Amplifier-Discriminator. A procedure found in the operator's manual was followed to aid in setting the



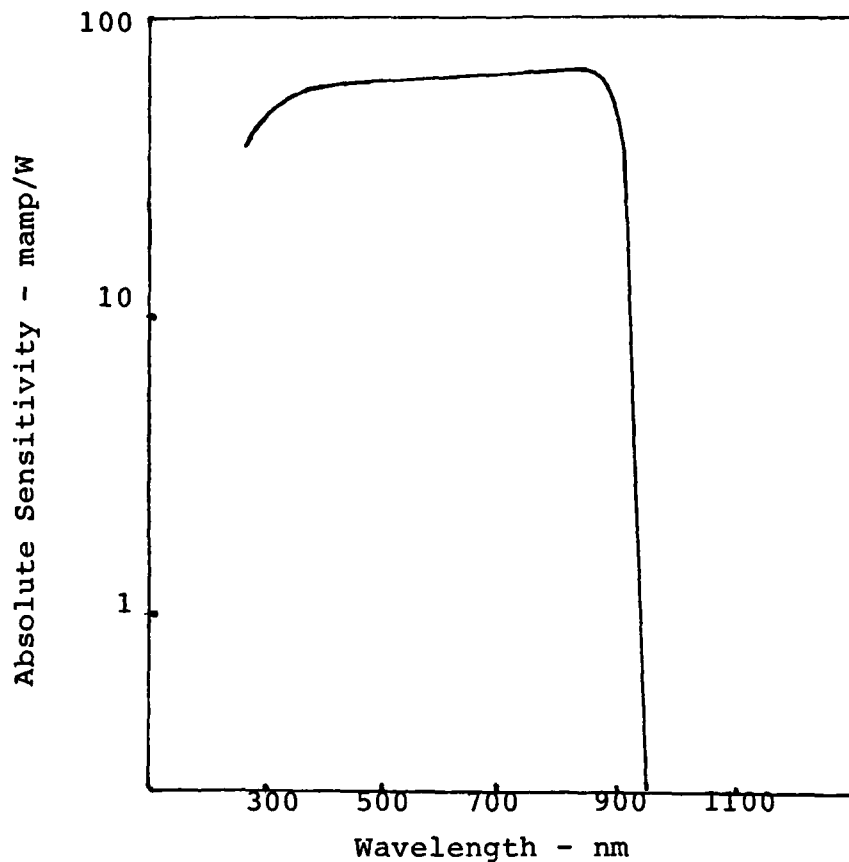


Fig. 12 RCA C31034 spectral response characteristics.

threshold controls for this unit and adjusting the PMT high voltage for optimum signal to noise. Subsequent to this stage, the signal was dispatched to a Canberra 8100/e multi-channel analyzer (MCA). The MCA's channel advance was made synchronous with the spectrometer scan rate via an interface box. Scan rates, corresponding channel advance rates, as well as the number of channels in which data was collected were chosen based on signal intensity, statistical considerations, and resolution. The resolution of the system after electronic processing should be at least as good as

the spectrometer's resolution. The resolution obtained with the MCA was better than 0.3 meV/channel for all experimental runs.

2. Sample Environment. To decrease the occurrence of non-radiative transitions, the sample's temperature was made as low as possible. A particularly useful cryogenic tool was the Janis Research Company's Detachable Tail Research Dewar. A schematic drawing is shown in Fig. 13.

The dewar consisted of a nitrogen and helium reservoir with capacities of four and two and one-half liters, respectively. Both reservoirs were surrounded by vacuum walls which acted as good insulators. The liquid nitrogen effectively served to provide a very cold external environment for the liquid helium so that it would not boil away immediately. The sample was cooled by either coming in contact with liquid, or just-vaporized, helium. It was preferable, though, not to immerse this sample in the liquid helium. If immersed, the turbulent boiling helium which moved across the sample would interfere with the outgoing luminescence. This degraded the statistical quality of the data and ultimately the resolution.

To prepare a thermally stable sample environment at very low temperatures, the following procedures were practiced.

- 1.) A mechanical pump was used to evacuate the outer jacket to about  $10^{-3}$  torr by opening the butterfly valve at A.

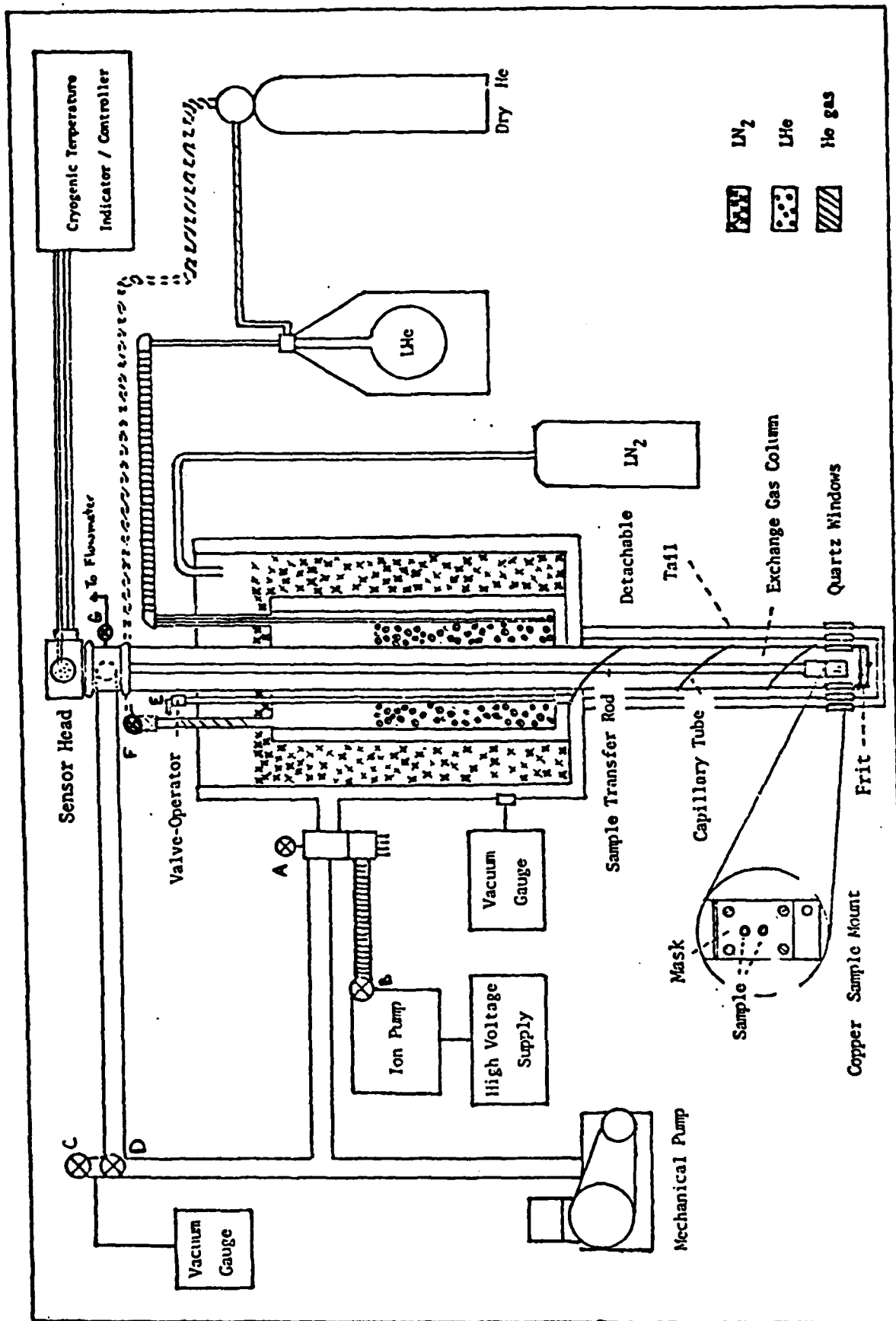


Fig. 13 Cryogenic and evacuation system

- 2.) Once this was accomplished, a fore pump followed by a diffusion pump further evacuated the jacket to  $10^{-6}$  torr by opening valve B and closing the butterfly valve A.
- 3.) Just prior to the addition of liquid nitrogen to its reservoir, it was imperative that all air, including water vapor, was purged from the helium space and the sample chamber. Thus, valve D and the needle valve, E, were opened. The needle valve controlled the flow through the capillary tube connecting the helium reservoir and sample column. Thus, the entire helium space was evacuated and freed of air which could freeze at liquid helium temperature. If air remained in the capillary tube, it would become blocked, prohibiting sample cooling during the experiment. Following the initial evacuation to approximately 0.1 torr, the helium space was filled with helium gas through valve F. As soon as a positive pressure of helium was attained, which would prevent any back-diffusion of air, valve F was closed. Positive pressure was observed by opening valve G. The space was subsequently re-evacuated as above. This procedure was repeated at least three times.
- 4.) One-half of the split cover at the top of the dewar was removed and liquid nitrogen added. The level of liquid nitrogen was continuously checked to ensure that the entire helium reservoir was covered. This should be continued for about four or five hours; the longer the better.
- 5.) Finally, the liquid helium was transferred to the helium reservoir following one last helium space purge as in step 3 above. Valve G should be open during the transfer. The helium reservoir was full when an opaque plume exited the exhaust tube of the reservoir.
- 6.) The sample was cooled to the desired temperature. Valves G and E were adjusted to maintain a stable temperature throughout the run.

The samples were mounted onto a copper block by means of two thin copper sheets. The bottom sheet consisting of two square apertures cut into the face to accommodate the samples was placed on the block first. The samples were

subsequently placed into the apertures. The top sheet was marked by two circular apertures, 3 mm in diameter. This sheet was placed on top of the other so that the circular openings overlaid the center of each sample. The two sheets were fastened to the copper block without straining the samples. It is known from solid state theory that such strain will affect the band gap.

A temperature sensing diode and heater were also connected to the copper block. The Lakeshore Cryotronics temperature controller monitored the sample temperature and provided power for the heater if needed. Sample temperatures were maintained at between roughly 4.5 and 7.5°K. These were approximate due to slight problems with the temperature indicator. Temperatures up to 7.24°K were recorded by the sensor when immersed in liquid helium.

### C. Electrical Measurements - Systems and Procedures

The following provides a summary of the equipment and procedures used for the electrical measurements. The equipment was located at the Air Force Avionics Laboratory.

1. C-V Profiling. The Hewlett-Packard Model 4061A Semiconductor/Component Test System was used in conjunction with an MSI Electronics Mercury Probe to obtain the C-V profiles. The Mercury Probe offered a means of producing and then removing non-destructively two closely spaced metal contacts to a semiconductor surface. The wafer

was placed face down on to the chuck shown in Fig. 14, covering the orifices. Liquid mercury was elevated from an underlying reservoir, up through the orifices, so that it made contact with the semiconductor. Differential voltage was applied incrementally across the mercury contacts. Subsequent measurements and calculations were performed by the Model 4061A Test System and computer resources provided by the Avionics Laboratory.

2. Hall Measurements. The theory summarized in Chapter II included with it a basic methodology for conducting Hall measurements. The system available at the Avionics Lab for such measurements is semi-automated. A system diagram is shown in Fig. 15.

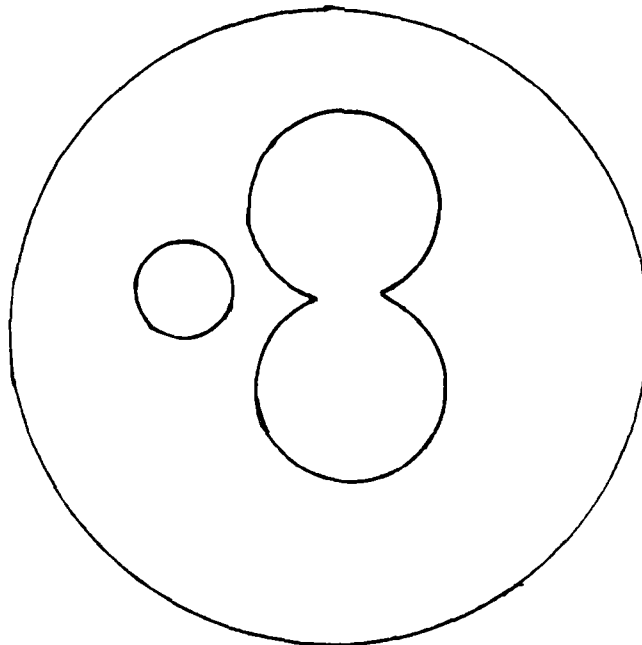


Fig. 14 Geometry of double column contacts.

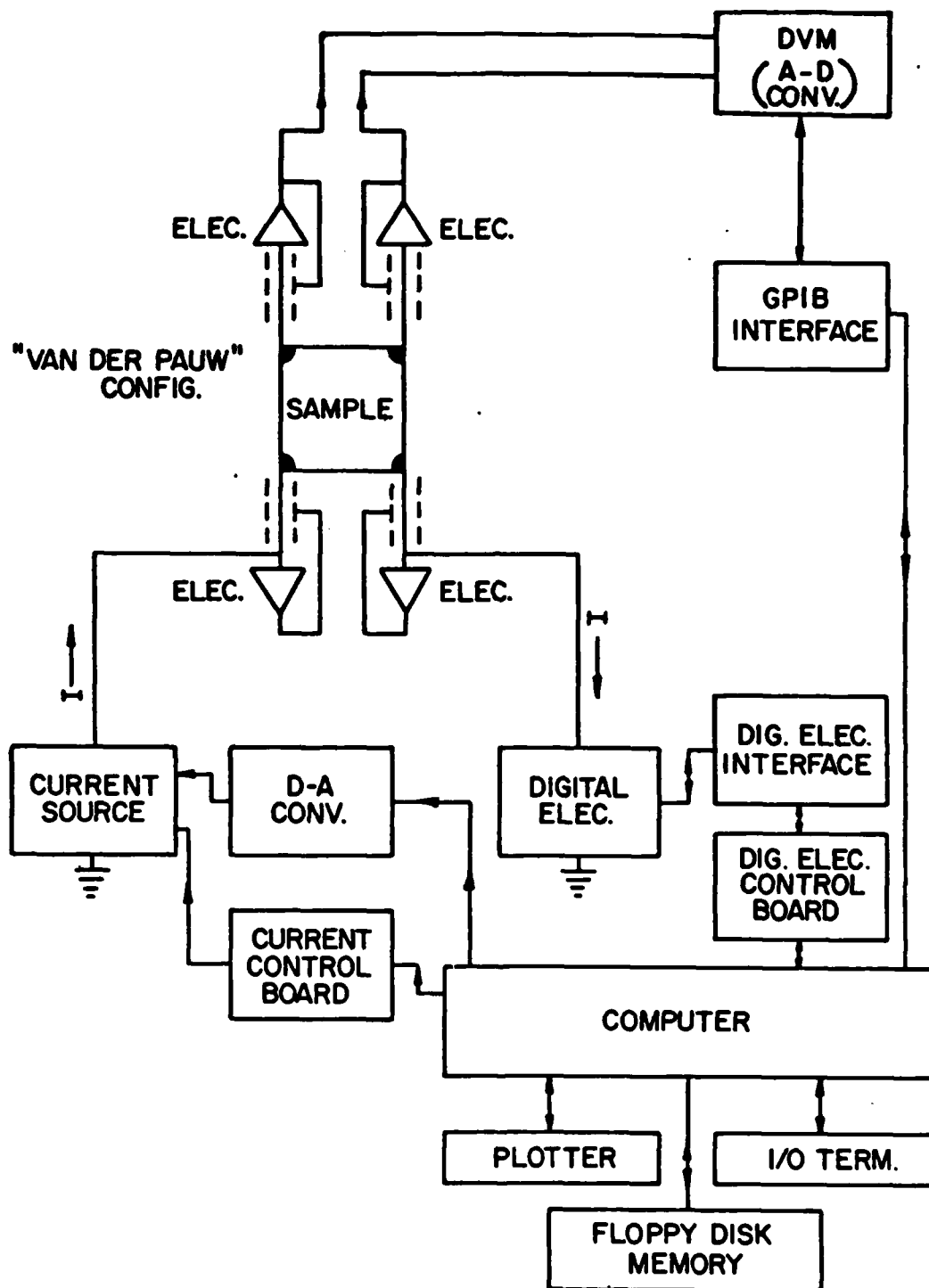


Fig. 15 Block diagram of automated Hall-effect/  
Sheet-resistivity measurement system (9:17).

#### IV. Results and Discussion

This section has been organized in a manner which aids in assigning spectral lines to transitions as well as in the final determination of the effect that implanted oxygen has on silicon implanted GaAs. Control samples are discussed and analyzed first. These include LEC grown GaAs, silicon implanted LEC GaAs and oxygen implanted LEC GaAs. Then the results for the silicon and oxygen implanted LEC GaAs are presented.

##### A. Characterization of Control Samples

There were three categories of control samples. First, the LEC GaAs substrate was electrically and optically characterized. Analysis of its photoluminescence spectrum isolated effects due to residual impurities in the LEC crystal. Second, substrates were implanted with silicon, at a dose,  $\phi$ , of  $6 \times 10^{12} \text{ cm}^{-2}$  and an energy of 100 keV. They were subsequently capped and annealed as outlined in the sample preparation section. These control samples were necessary to highlight the effects due to the silicon implantation and the capping and annealing (C/A) steps. Finally, substrates were implanted with oxygen,  $\phi = 3 \times 10^{12} \text{ cm}^{-2}$  or  $\phi = 1.5 \times 10^{12} \text{ cm}^{-2}$  and an energy of 65 keV. Some were subjected to the same heat treatment and, if required, capping procedure that was planned following oxygen implantation of the silicon



implanted GaAs. Thus, the effects associated with oxygen itself and those due to C/A, or just annealing, could be delineated.

### 1. LEC GaAs.

1a. C-V Measurements. It was already suspected that the substrates used in this investigation were semi-insulating, i.e. neither n- or p- type. This was quickly verified with a C-V measurement. There was essentially no measureable carrier profile, indicating negligible carrier concentration.

1b. Luminescence Measurements. The PL spectrum for the substrate is shown in Fig. 16.

The first two peaks are due to excitonic transitions. Their energy and assignments are listed below (17):

<u>Line (eV)</u>	<u>Assignment</u>
1.5152	Free exciton
1.5124	Exciton bound to neutral acceptor

Ashen, et.al., (43) assigned carbon as the neutral acceptor in the 1.5124 eV transition. This correlates well with the residual carbon impurities that are generally found in LEC grown crystals.

The statistical scatter in the data makes assignment of peaks in the shallow acceptor band difficult. Just preceding the large band is a small shoulder at 1.5058 eV. Kunzel and Ploog assign this to an exciton bound to a point

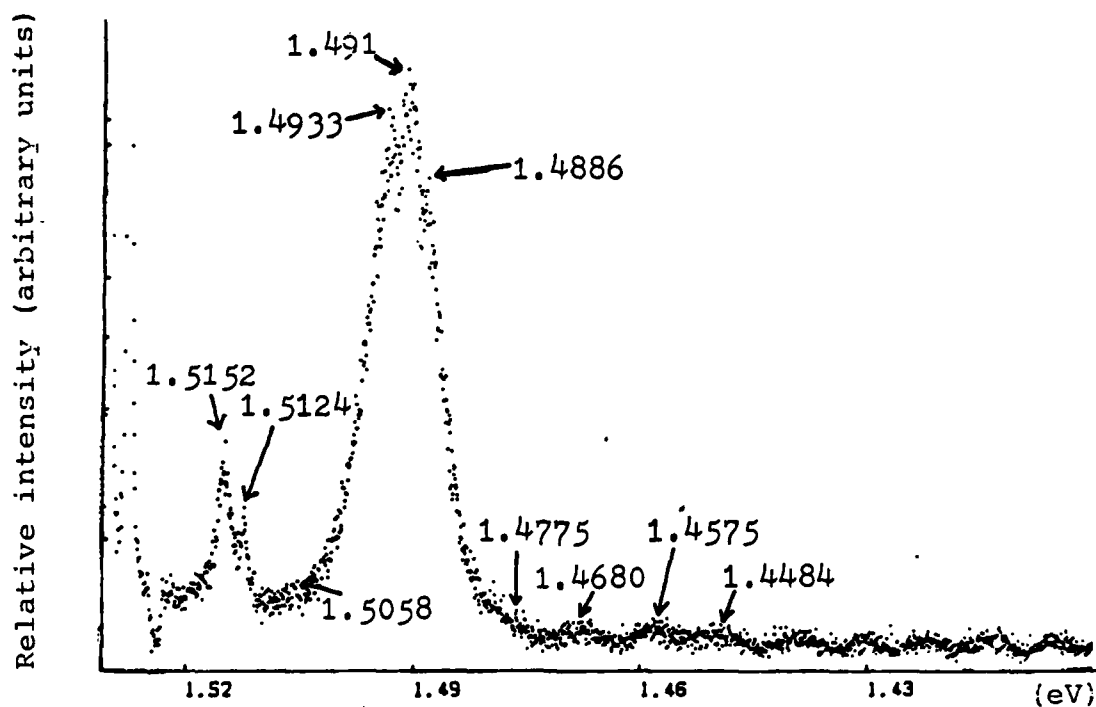


Fig. 16 PL of LEC GaAs at 5°K using 4880 Å line.  
Source Intensity: 10 W/cm .

defect such as a Ga vacancy (44:417). The possibility that these particular crystals might have a high native defect concentration could be interfering with the data's quality. The following peaks constitute the acceptor band:

<u>Line (EV)</u>	<u>Assignment</u>
1.4933	(e,C <sub>As</sub> ) free-electron, carbon acceptor transition
1.4910	(D,C <sub>As</sub> ) neutral donor, carbon acceptor pair transition
1.4886	Zinc acceptor ( ? )

Although the peak at 1.4886 eV has been assigned to the zinc acceptor (43), the presence of Zn is doubtful because the impurity is generally not found residually in LEC grown GaAs. Therefore, further analytical techniques, such as secondary ion mass spectrometry (SIMS), is needed for positive identification.

A striking feature of the substrate luminescence was the existence of several equally spaced, broad, low intensity peaks. They started at 1.4775 eV and were spaced approximately 9 meV apart. The first peak may correspond to the LO phonon replica of the bound exciton transition at 1.5124 eV. This is based on the fact that 36 meV corresponds to the LO phonon coupling energy in GaAs. Interestingly, the transverse acoustic (TA) phonon energy in GaAs is 9 meV (14:388). However, the supposition that these repetitive peaks may be associated with TA phonons is disputed by the fact that TA coupling is highly unlikely (14:388).

## 2. Silicon Implanted LEC GaAs.

2a. C-V and Hall Measurements. Both C-V profiles and electrical Hall measurements were obtained for the silicon implanted samples. A representative profile is shown in Fig. 17.

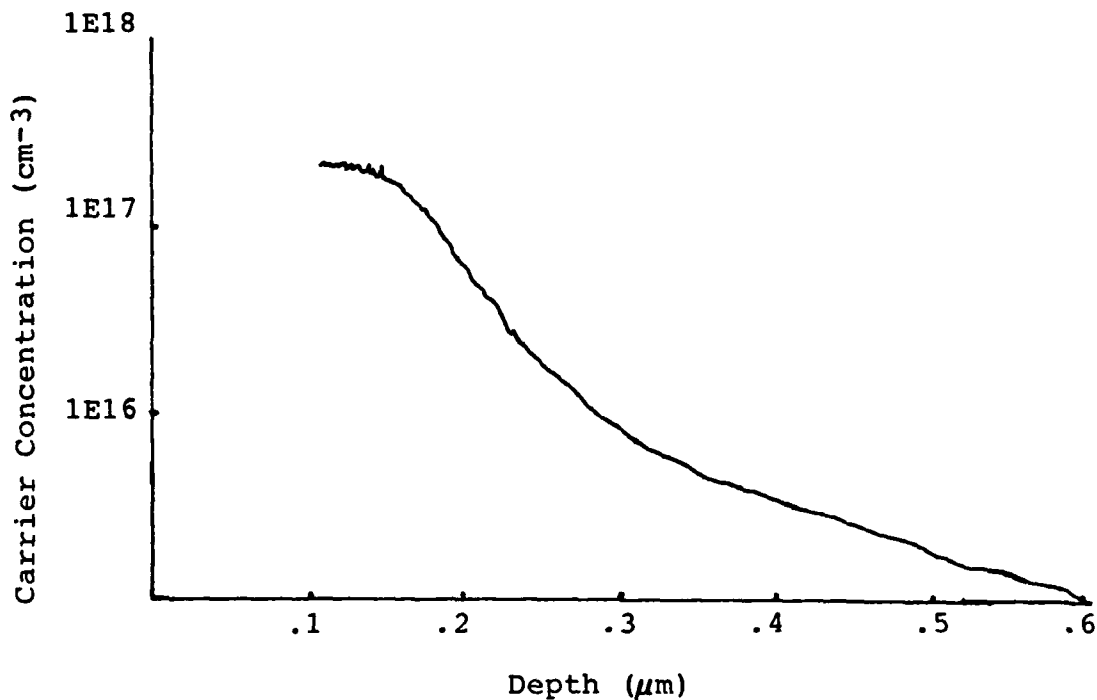


Fig. 17 Typical C-V profile for Si-implanted GaAs at  $\phi = 6E12$  and  $E = 100$  keV.

As can be seen in Fig. 17, the peak carrier concentration was about  $3.5 \times 10^{17} \text{ cm}^{-3}$  at a depth of  $.11 \mu\text{m}$ . The

electrical measurements, reported earlier, found  $N_S$  to be  $2 \times 10^{12} \text{ cm}^{-2}$  and  $\rho_S$  to be  $6.68 \times 10^2 \Omega/\square$ .

2b. Luminescence Measurements. The PL spectrum for silicon implanted LEC GaAs, using the argon laser as an excitation source, is shown in Fig. 18. With this laser, the crystal is being "illuminated" to a depth approaching that of the peak carrier concentration. (See Table I) Readily apparent are the excitonic recombinations at 1.5141 and 1.5128 eV. It appears that the silicon has given rise to the 1.5141 eV peak, which has been categorized as due to an exciton bound to a neutral donor (17). The 1.5128 eV peak corresponds to the previously mentioned 1.5124 eV line. The character of the acceptor band has not changed significantly from that presented in Fig. 16 for the substrate. However, the  $(e, C_{AS})$  transition appears to have diminished relative to the  $(D, C_{AS})$  transition after silicon implant. In addition, the peak at 1.4880 eV, corresponding to the previously mentioned 1.4886 eV line, has gained stature following the silicon implantation.

The effect of temperature variation on the luminescence is illustrated in Fig. 19. Most noticeable is the change in the relative intensities of the 1.4939 eV  $(e, C_{AS})$  and the 1.4903 eV  $(D, C_{AS})$  peaks. As expected from theory, the donor-acceptor transition gradually diminishes with increasing temperature as fewer donors remain neutral. Another interesting point is that the intensities of the

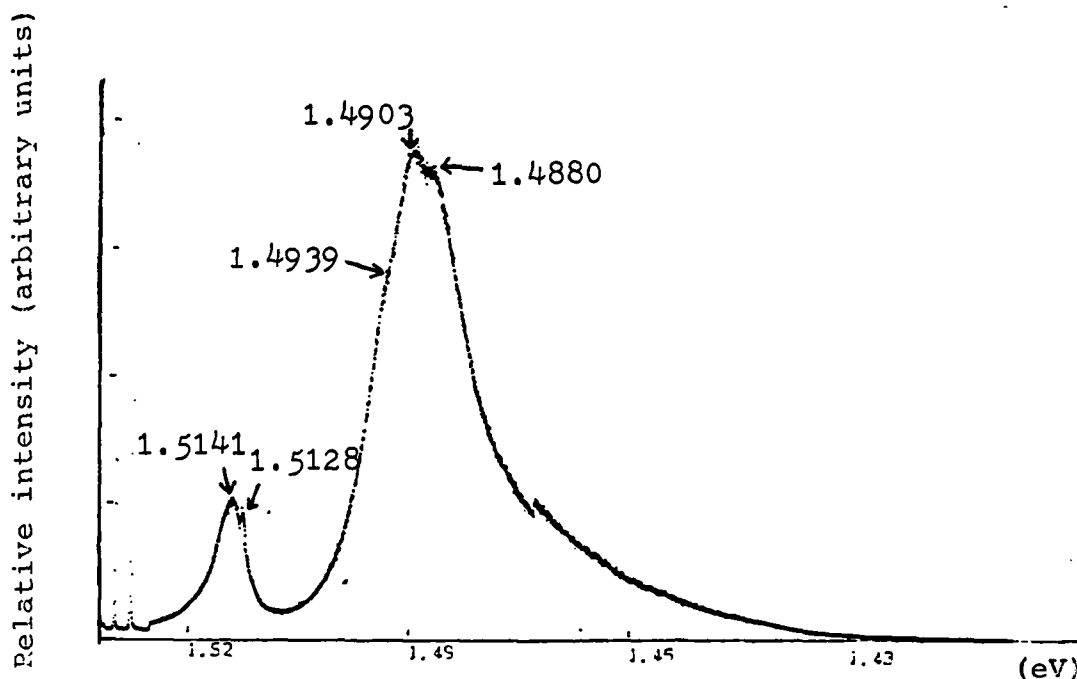


Fig. 18 PL of Si-implanted GaAs at 5°K using 4880 Å line. Source intensity: 20W/cm<sup>2</sup>.

1.4903 and 1.4880 eV lines change similarly with temperature. It has been theorized that the energy binding an exciton to an ionized donor is 1.06 times the donor ionization energy (17) and more donors become ionized as the temperature is increased. Therefore, it is reasonable to presume that the

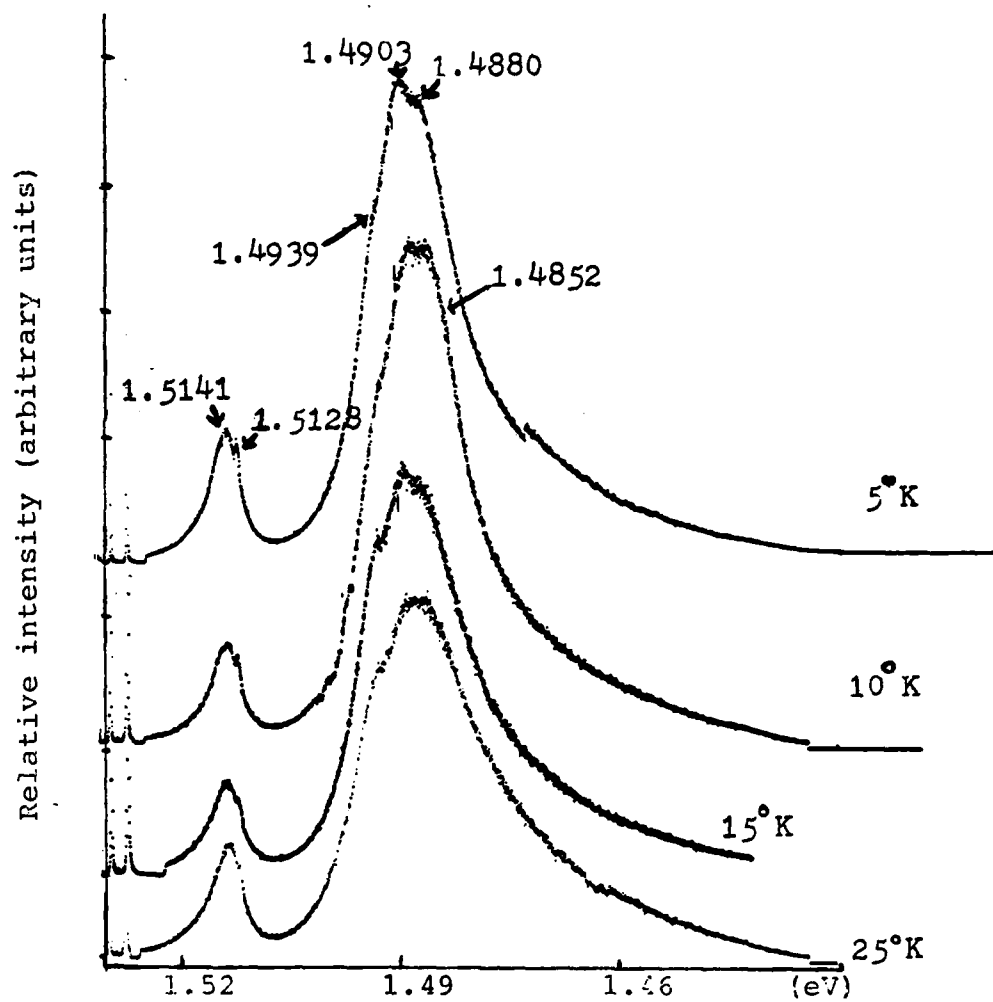


Fig. 19 PL of Si-implanted GaAs at different sample temperatures using 4880 Å line. Source intensity: 20 W/cm<sup>2</sup>.

intensities of the lines associated with the bound exciton ionized donor transition and donor-acceptor transition would diminish equally with increasing temperature, as shown in Fig. 19. This lends support to the assignment of the 1.4880 eV line as an exciton bound to an ionized donor (17). It is interesting to note also that the 1.4852 eV line attributed to silicon acceptors has emerged (43).

The final characterization undertaken for the silicon implanted substrates was near-surface layer luminescence using the krypton laser. The PL spectra as a function of depth are shown in Fig. 20. At the surface, the acceptor band has a broadened low energy tail and at least one peak is apparent at 1.464 eV. This structure corresponds to the Q-band associated with silicon implanted GaAs (26). The native defects associated with the Q-band depend upon the implantation process, the capping conditions, and silicon dose. The low dose present in this investigation probably accounts for its weak intensity. Most interesting is the existence of the small shoulder at 1.4862 eV which is present in spectra taken from the surface into a depth of 1264 Å. This shoulder has been associated with free electron recombination at a  $\text{Si}_{\text{As}}$  acceptor site ( $\text{e}, \text{Si}_{\text{As}}$ ) (45).

### 3. Oxygen Implanted LEC GaAs.

3a. Luminescence Measurements. Substrates were implanted with oxygen at  $\phi = 1.5 \times 10^{12} \text{ cm}^{-2}$  and  $\phi = 3 \times 10^{12} \text{ cm}^{-2}$  and at an energy of 65 keV. It was



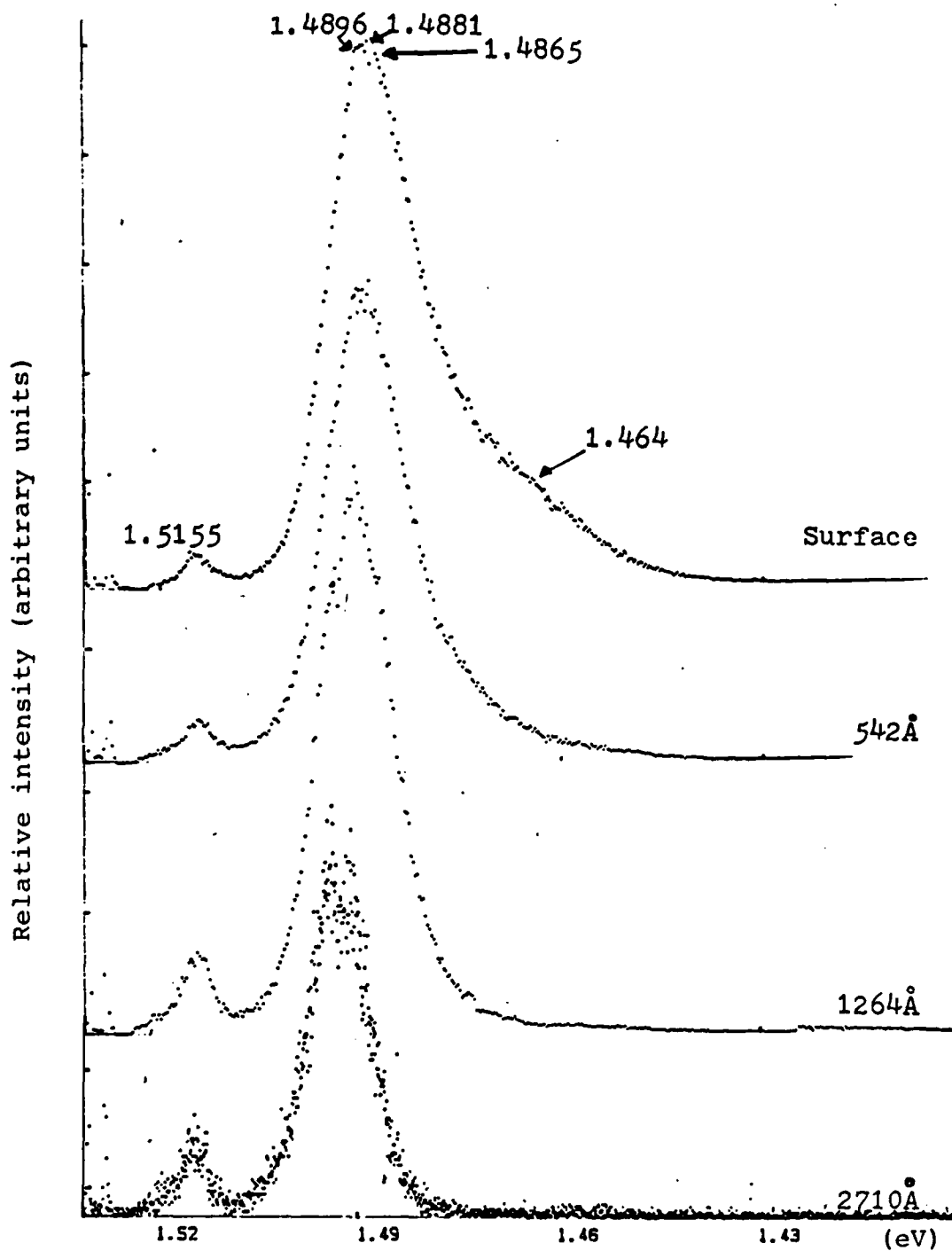


Fig. 20 Spectra of Si-implanted GaAs at 5.5°K using 3500 Å line. Source intensity: 5.5 W/cm<sup>2</sup>.

suspected and found early that the higher dose produced lower PL intensity due to the additional crystal damage. Therefore, the high dose implanted samples were not pursued extensively.

An argon laser was used to illuminate a non-annealed oxygen implanted substrate. Excitation intensity was  $18 \text{ W/cm}^2$ . Also a Krypton laser, with an intensity of  $5 \text{ W/cm}^2$ , excited a similarly implanted crystal which had undergone a heat treatment of  $400^\circ\text{C}$  for two hours. This sample was etched to  $600 \text{ \AA}$ . Both spectra (not shown), similar in appearance, had low integrated intensity. Therefore the search for any oxygen-related peaks was hampered. However, the carbon-related acceptor peaks were still present.

Fig. 21 shows the PL spectra for an oxygen implanted substrate, but one which was capped and annealed at  $900^\circ\text{C}$  for 15 minutes. The sample was subjected to near-surface luminescence via a krypton laser excitation source. The integrated intensity is at least an order of magnitude greater than that achieved with the previously mentioned oxygen implanted samples. After annealing at  $900^\circ\text{C}$ , excitonic transitions which were seen in the substrate and the silicon implanted samples, are visible. Most noteworthy is the  $1.5143 \text{ eV}$  line, which was previously attributed to silicon. Also visible is a shoulder at  $1.5059 \text{ eV}$  which again may indicate the existence of point

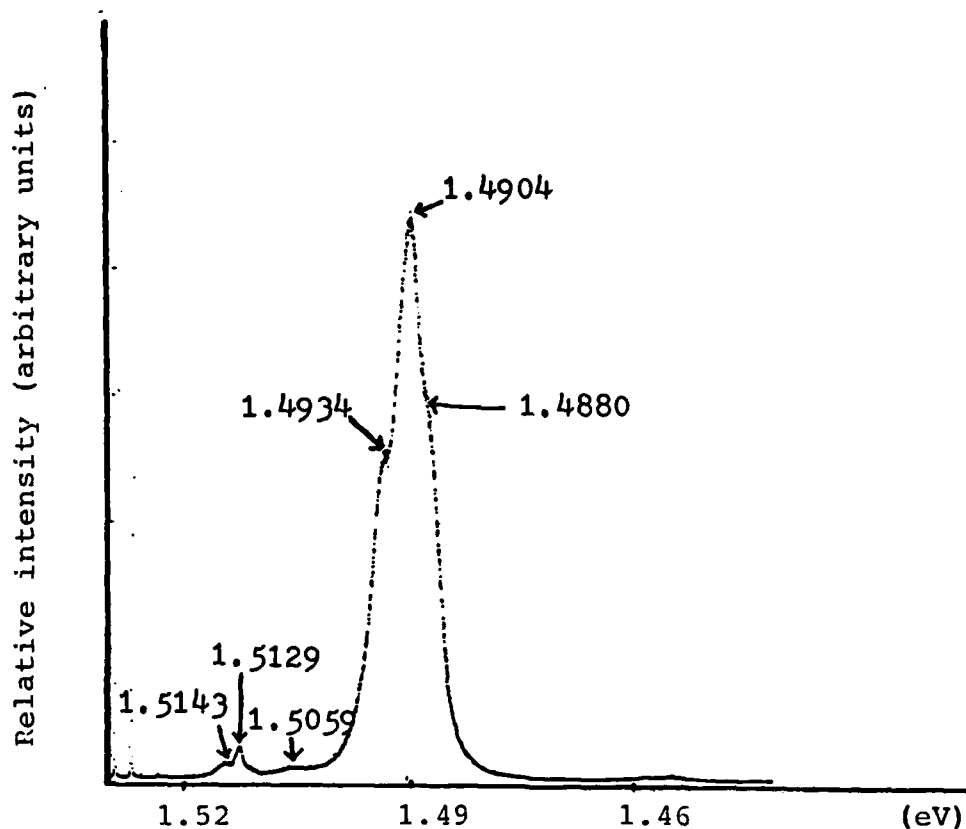


Fig. 21 PL of O-implanted GaAs at 5.5°K using 3500 Å line. Source intensity: 5.5 W/cm<sup>2</sup>.  
T<sub>A</sub> = 900°C for 15 min.

defects such as Ga vacancies. Sydenstricker (46:IV-23) also found such results and attributed these defects to the annealing procedure. In contrast to the near surface luminescence for silicon implanted GaAs, there is no low

energy tail associated with the acceptor band in this case. Thus, the Q-band defects are not created by the implantation of oxygen alone or the subsequent C/A procedures. The  $C_{As}$ -related peaks may obscure the presence of possible O-related peaks.

#### B. Characterization of Silicon and Oxygen Implanted Gallium Arsenide

As stated before, oxygen was implanted at a dose of  $1.5 \times 10^{12} \text{ cm}^{-2}$  or  $3 \times 10^{12} \text{ cm}^{-2}$ , which was either one-half of, or equal to,  $N_S$  of the silicon implanted GaAs (GaAs:Si) samples. The following data was accumulated for both doses after annealing at temperatures ( $T_A$ ) of 400 and 900°C subsequent to oxygen implantation.

1. Electrical Measurements. The results of the surface electrical measurements are shown in Table III, including those of the silicon implanted substrate for comparison. The average sheet resistance of the GaAs:Si sample increased about four orders of magnitude after implanting oxygen and annealing it at 400°C for two hours. However, the sheet resistance increased by only a factor of 1.5 when a similarly implanted sample was subsequently annealed at 900°C.

Table III

## Surface Electrical Measurements for Silicon and Oxygen Implanted GaAs

Implant	Dose ( $\text{cm}^{-2}$ )	Energy (keV)	$T_A$ ( $^{\circ}\text{C}$ )	$\rho_s$ ( $\Omega/\square$ )
Silicon	$6 \times 10^{12}$	100	850	$6.68 \times 10^2$
* Silicon + Oxygen	$1.5 \times 10^{12}$	65	400	$1.09 \times 10^6$
* Silicon + Oxygen	$3 \times 10^{12}$	65	400	$4.9 \times 10^5$
* Silicon + Oxygen	$1.5 \times 10^{12}$	65	900	$9.0 \times 10^2$
* Silicon + Oxygen	$3 \times 10^{12}$	65	900	$8.4 \times 10^2$

\* The dose, energy and  $T_A$  shown in this line refers to the oxygen implant. Silicon was implanted as per line one in all cases.

2. Luminescence Measurements. The spectral character of the  $400^{\circ}\text{C}$  annealed samples resembles very closely that of the semi-insulating substrate. This is noteworthy in and of itself. Fig. 22 illustrates this very well. In addition, the layered PL characterization of the low dose oxygen implant reveals an interesting feature. For depths up to and slightly in excess of the projected range for the silicon and oxygen implants, the  $(e, C_{AS})$  and  $(D, C_{AS})$  recombinations occur about equally. However, at about  $2100 \text{ \AA}$  a change is observed. As the depth increases, the free-to-bound,  $(e, C_{AS})$ , recombination emission intensity

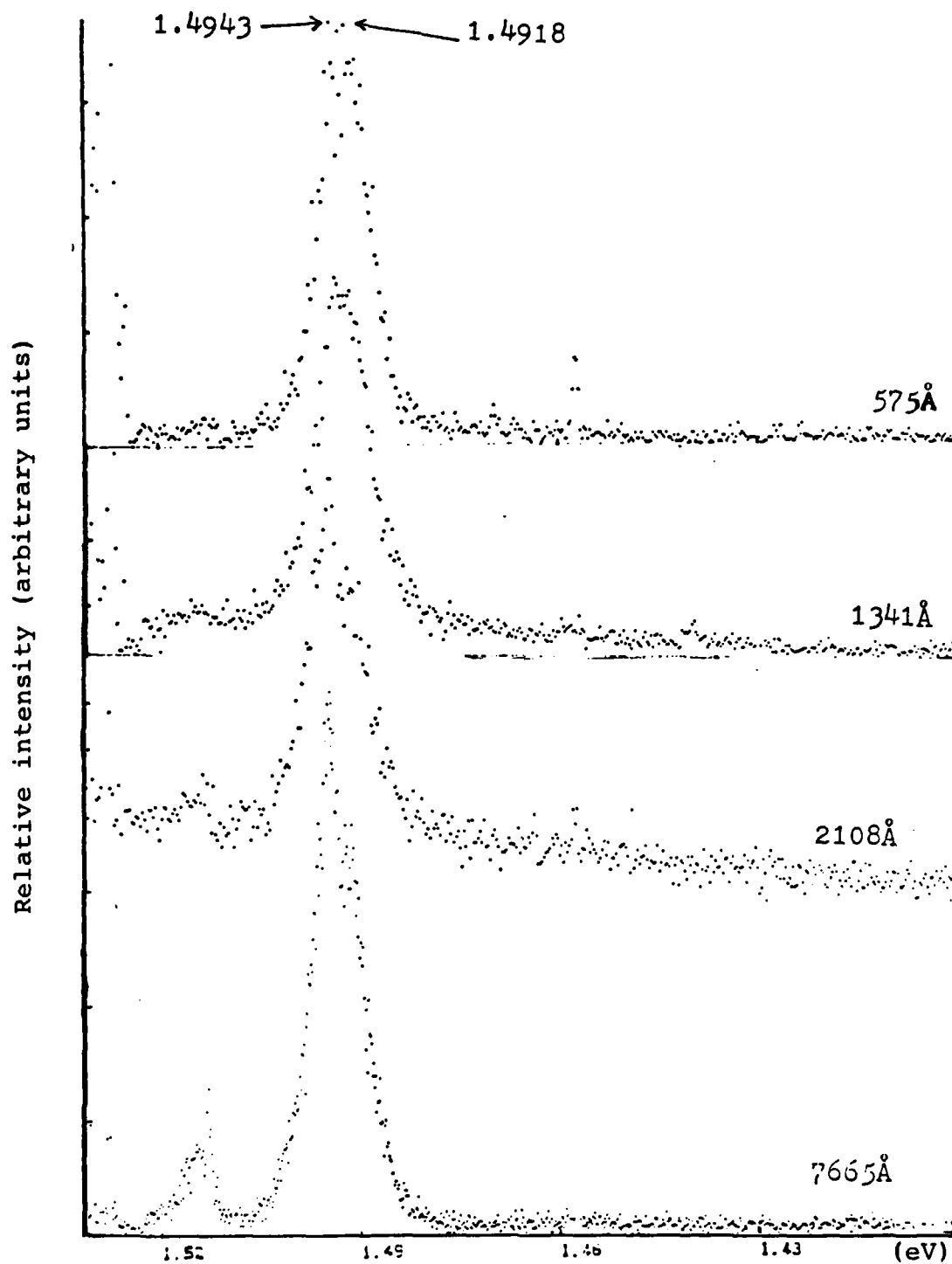


Fig. 22 PL etch spectra of O-implanted GaAs:Si at 5-8 K using 3500 Å line. Source intensity: 5.5 W/cm<sup>2</sup>. O dose:  $1.5 \times 10^{12}$  cm<sup>2</sup>, E = 65 keV. T<sub>A</sub> = 400°C for 2 hrs.

increases beyond that of the donor-acceptor pair transition as also shown in Fig. 23. Thus, it is possible that the oxygen and/or implant related defects partially compensate the free electrons. The distribution of induced defects discussed in Chapter II would account for the partial compensation slightly beyond the projected range of the oxygen implants. Finally, the intense peak associated with  $(e, Si_{As})$ , found in GaAs:Si layers, is not observable in these spectra. It is speculated, therefore, that oxygen may be creating intermediate levels within the band gap. As a result, electrons recombine with valence band holes via these newly created levels rather than through the acceptor level associated with  $Si_{As}$ . This would explain the disappearance of the  $(e, Si_{As})$  peak. This intermediate level may also explain the behavior of the  $(e, C_{As})$  peak discussed above. The relative intensity of this peak grew rapidly at depths beyond the depth of the peak oxygen concentration, i.e. beyond the depth at which the oxygen associated intermediate level would presumably be most likely. Similar comments can not be put forth for the sample containing  $3 \times 10^{12} \text{ cm}^{-2}$  dose due to the lack of sufficient layered luminescence data. However, to a depth of  $2124 \text{ \AA}$ , its spectral characteristics (not shown) closely resemble those for the lower dose.

Fig. 24a depicts the Q-band found in GaAs GaAs:Si (26). Alongside, Fig. 24b shows the PL characteristics, in

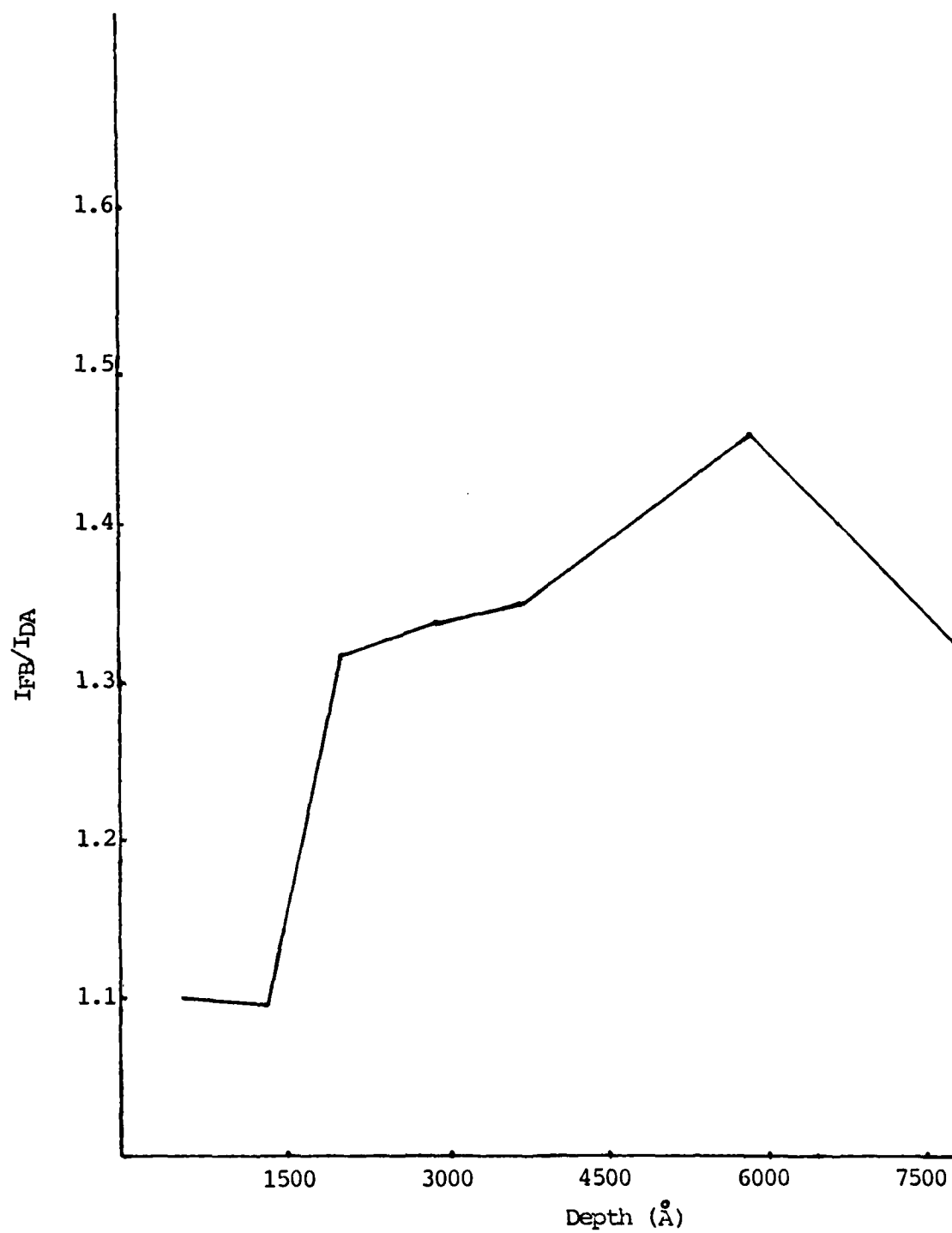
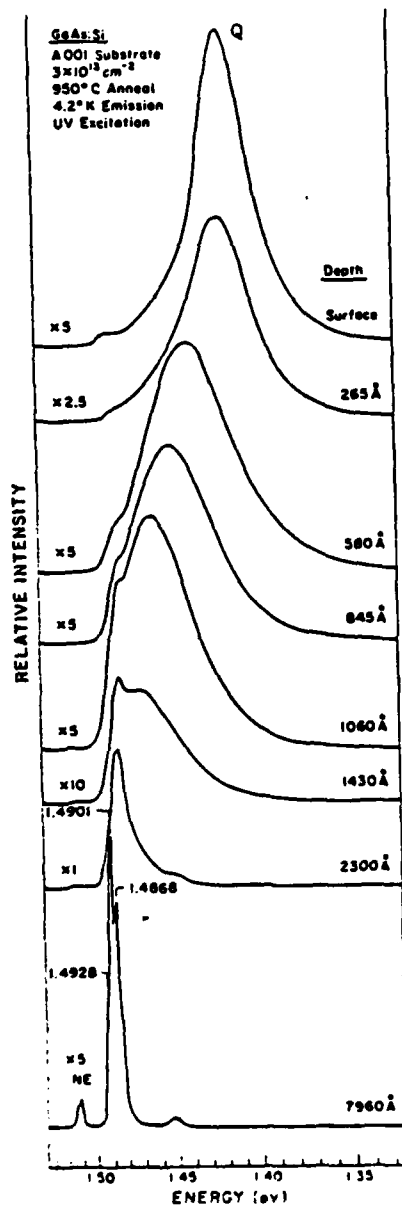
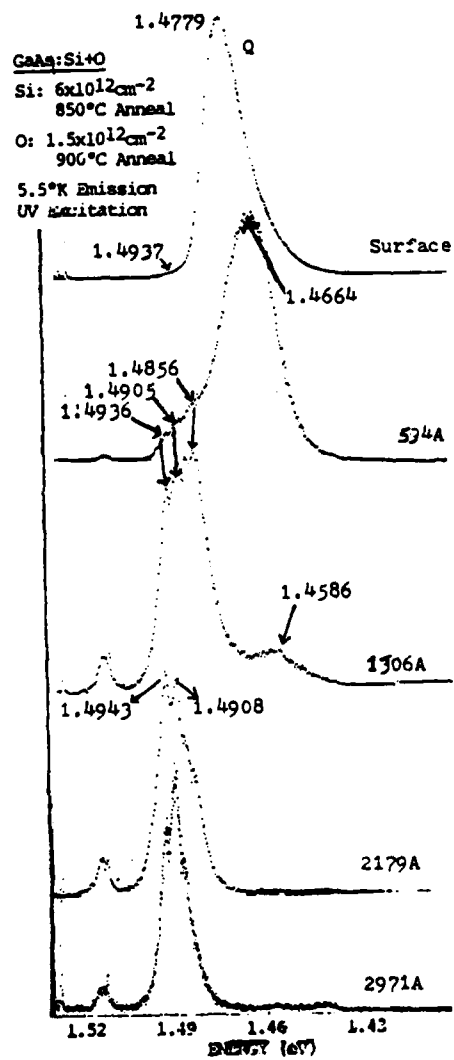


Fig. 23 Ratio of free-to-bound to donor-acceptor pair recombination intensities vs. depth.





a.



b.

Fig. 24 Q-band observed in (a) GaAs:Si layers (26) and (b) GaAs:Si+O layers.

particular the Q-band, of the  $1.5 \times 10^{12} \text{ cm}^{-2}$  oxygen implanted GaAs:Si (GaAs:Si+O) after a  $900^\circ\text{C}$  anneal. The Q-band of the GaAs:Si shifts monotonically to higher energy with depth, while that of GaAs:Si+O shifts first to lower then to higher energy. If one returns to the discussion concerning the silicon implanted GaAs control samples (Fig. 20), the low Q-band intensity was attributed to the relatively low silicon dose of silicon. With the addition of oxygen, the Q-band's relative intensity has increased greatly. One must also recall in the discussion of PL characteristics for oxygen implanted substrates (Fig. 21), that the Q-band was not present. Thus, the oxygen, it is hypothesized, must be assisting in the formation of complexes involving silicon, closely related to those suitable for the Q-band. It is conceivable that oxygen itself is a component of one of the defect-related complexes often associated with the Q-band.

The strong  $\text{Si}_{\text{As}}$  peak (at 1.4856 eV), observed previously in the GaAs:Si layers, is also present in Fig. 24. It appears that oxygen is not as readily available to form intermediate levels described previously for the  $400^\circ\text{C}$  annealed O-implanted GaAs:Si layers. Thus, the electrons once again transit the band gap via the acceptor level associated with  $\text{Si}_{\text{As}}$ .

Fig. 25 shows the layered PL characteristics for an oxygen dose of  $3 \times 10^{12} \text{ cm}^{-2}$ . It appears that the

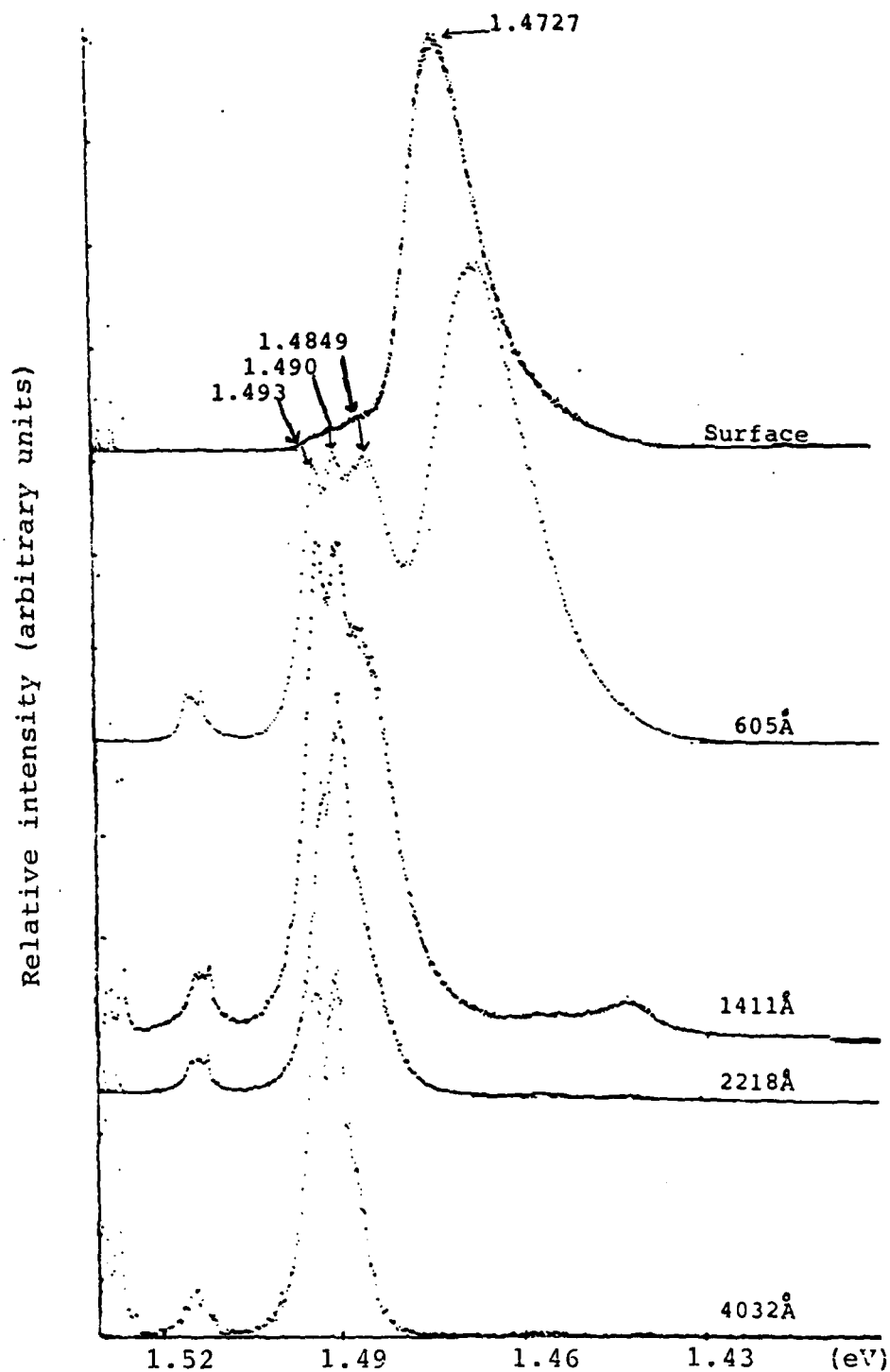


Fig. 25 PL etch spectra of O-implanted GaAs:Si at 5-8°K using 3500 Å line. Source intensity: 5.5 W/cm<sup>2</sup>. O dose:  $3 \times 10^{12}$  cm<sup>-2</sup>, E = 65 keV. T<sub>A</sub> = 900°C for 15 min.

increased oxygen dose has little effect except perhaps in the rate with which the intense band disappears with depth. This is especially apparent from the emergence of well-resolved, relatively narrow peaks, such as that due to the silicon acceptor, at a depth of 600 Å.

In summary, at anneal temperatures of 400°C, the luminescence characteristics of the GaAs:(Si+O) layers are much like those of the substrate itself. Also, the strong Si<sub>As</sub> peak, found in the GaAs:Si layers, disappeared suggesting the creation of O-associated intermediate levels within the band gap. After annealing similarly implanted layers at 900°C, oxygen appeared to assist in the formation of Q-band related complexes involving silicon, rather than in the creation of intermediate levels within the band gap. The fact that the Q-band was neither present in the 400°C annealed GaAs:(Si+O) layers nor the 900°C capped and annealed O-implanted substrates leads one to conclude that such Q-band related complexes are strongly dependent upon a sufficient concentration of silicon and use of C/A procedures.

## V. Conclusions and Recommendations

### A. Conclusions

This, to the best of my knowledge, is the first photoluminescent characterization of GaAs:Si+O. It was found that there was some correlation between the electrical and optical properties of these layers. Spectral features found in the Si-implanted layers included a prominent free-to-bound  $\text{Si}_{\text{As}}$  acceptor peak as well as the Q-band. The  $\text{Si}_{\text{As}}$  acceptor peak and Q-band were not observed in the 400°C annealed GaAs:Si+O layers, which had very high electrical activity. However, both the  $\text{Si}_{\text{As}}$  acceptor peak and a much enhanced Q-band were readily apparent in the GaAs:Si+O layers annealed at 900°C, which had relatively low electrical resistivity. It was, therefore, hypothesized that intermediate levels had been created by oxygen in the 400°C annealed samples. The re-emergence of the  $\text{Si}_{\text{As}}$  acceptor peak in the 900°C annealed samples suggests the absence of these intermediate levels. In addition, the appearance of a greatly enhanced Q-band indicates that oxygen might aid in the formation of the complexes giving rise to this band, rather than creating intermediate levels.

### B. Recommendations

1.) In order to strengthen the optical/electrical data correlation, further experimentation is required to

substantiate the hypothesized intermediate levels. This would require slightly altering the current experiment in order to scan the low energy spectral region (0.5 - 1.0 eV). In addition it is desirable to better characterize the Q-band found in the 900°C annealed, GaAs:Si+O layers. This would include the correlation of this peak's intensity to those associated with the possible intermediate levels.

2.) A differently grown crystal should be chosen. In addition to the near edge residual peaks, it has been reported that the LEC grown substrate has associated photoluminescence peaks at 0.65, 0.67, and 0.8 eV, which would interfere with the proposed intermediate level characterization (47:484). It is suggested that an epitaxially grown crystal be selected for further photoluminescence studies.

3.) Further data are needed on different anneal temperature, implantation doses and energy to better correlate the electrical and optical behavior of GaAs:Si layers which have been implanted with oxygen.

### Bibliography

1. Mills, T. G. "Gallium Arsenide Technology for High Frequency Analog and High Speed Digital Applications," Quest, 4: 22-41 (Spring 1980).
2. Foyt, G. A., et. al. "Isolation of Junction Devices in GaAs Using Proton Bombardment," Solid State Electronics, 12: 209-214 (1969).
3. Gossick, B. R. "Disordered Regions in Semiconductors Bombarded by Fast Neutrons," Journal of Applied Physics, 30: 1214-1218 (August, 1959).
4. Stephens, K. G. and B. J. Sealy. "Use of Ion Implantation in Future GaAs Technology," Microelectronics, J-9: 13-18 (1978).
5. Favennec, P. N., et. al. "Compensation of GaAs by Oxygen Implantation," Ion Implantation in Semi-Conductors 1973. 621-630 (1973).
6. Martin, G. M., et. al. "Effects of Oxygen Implantation in GaAs," Semi-insulating III-V Materials. 275-282. Evian, France 1982.
7. Favennec, P. N. "Semi-insulating layers of GaAs by Oxygen Implantation," Journal of Applied Physics, 47: 2532-2536 (June 1976).
8. Woods, J. F. and N. G. Ainslie. "Role of Oxygen in Reducing Silicon Contamination of GaAs During Crystal Growth," Journal of Applied Physics, 34: 1469-1475 (May 1963).
9. Pronko, P. P., et. al. "Ion Implantation in III-V Compound Semiconductors." Final Report to Avionics Laboratory, Air Force Systems Command. Contract F33615-80-C-1108 with Universal Energy Systems, Inc. Wright-Patterson AFB OH, September 1984.
10. Pronko, P. P. et al. Unpublished data obtained under Contract F33615-80-C-1108. See Ref. 9
11. McKelvey, J. P. Solid State and Semiconductor Physics. New York: Harper Row Publishers, 1966.
12. Gershezon, M. "Radiative Recombination in the III-V Compounds," Semiconductors and Semi-metals, 2, edited by R. K. Willardson and A. C. Beer. New York: Academic Press (1955).

13. Rickayzen, G. "The Validity of the Hydrogen-like Approximation for Impurity Levels," Journal of Electronics, 1: 122-125 (1955).
14. Bebb, H. Barry and E. W. Williams. "Photoluminescence II: Gallium Arsenide," Semiconductors and Semi-metals, 8, edited by R. K. Willardson and A. C. Beer. New York: Academic Press, 1967.
15. Pankove, J. I. Optical Processes in Semiconductors," Englewood Cliffs, Prentice-Hall, Inc., 1971.
16. Bebb, H. Barry and E. W. Williams. "Photoluminescence I: Theory," Semiconductors and Semi-metals, Volume 8, edited by R. K. Willardson and A. C. Beer. New York: Academic Press, 1967.
17. Bogardus, H. E. and Bebb, H. B. "Bound-Exciton, Free-Exciton, Band-Acceptor, Donor-Acceptor and Auger recombination in GaAs," Physical Review, 176: 993-1002 (15 December 1968).
18. Nam, S. B., et. al. "Free-exciton energy spectrum in GaAs," Physical Review B, 13: 761-767 (15 January 1976).
19. Sharma, R. S. and Rodriguez, S. "Exciton-Donor Complexes in Semiconductors," Physical Review, 159: 649-651 (15 July 1967).
20. Sharma, R. S. Rodriguez S. "Theory of Excitons Bound to Ionized Impurities in Semiconductors," Physical Review, 153: 823-827 (15 January 1967).
21. Stringfellow, G. B., et. al. "Photoluminescence of Carbon-Implanted GaAs," Applied Physics Letters, 39: 581-582 (15 October 1981).
22. Yu, P. W. and D. C. Walters "Deep Photoluminescence Band Related to Oxygen in Gallium Arsenide," Applied Physics Letters, 41: 863-865 (1 November 1982).
23. Emori, H. et. al. "Effect of Ambient Gas on Undoped LEC GaAs Crystal," Japanese Journal of Applied Physics, 22: 1652-1655 (November, 1983).
24. Yokogawa, M. et. al. "Effects of Whole Ingot Annealing on 1.49 eV PL Properties in LEC-Grown Semi-Insulating GaAs," Japanese Journal of Applied Physics, 23: L339-L341 (May, 1984).



25. Elliott, K. R. "Residual Double Acceptors in Bulk GaAs," Applied Physics Letters, a--: 274-278 (1 February 1983).
26. Pomrenke, G. S., et. al. "Luminescence Characteristics of the 1.4 eV Silicon Related Complex in Gallium Arsenide," Physica B+C, 116: 414-419 (1983).
27. Voltsit, V. V., et. al. "Photoluminescence of Gallium Arsenide Doped by Silicon Implantation," Soviet Physics Semiconductors, 12: 1211-1213 (October 1978).
28. Nahan, M. I. and Burns, G. "Recombination Radiation in GaAs," Physical Review, 129: 125-128 (1 January, 1963).
29. Devaud, B. and P. N. Favennec. "Levels Obtained by Oxygen Implantation in Gallium Arsenide," Institute of Physics Conference Series, No. 45: 492-500 (1979).
30. White, A. M. et. al. "Bound Exciton Luminescence Associated With the Deep Oxygen Donor in Gallium Arsenide," 1974 Proceedings of the 12th International Conference on the Physics of Semiconductors (Stuttgart:Teubner): 381-385 (1974).
31. Monemar, B. and Blum, J. M. "Optical Characterization of Deep O Implants in GaAs," Journal of Applied Physics, 48: 1529-1537 (April, 1977).
32. Chang, L. L. et. al. "Vacancy Association of Defects in Annealed GaAs," Applied Physics Letters, 19: 143-145 (1 September, 1971).
33. Kolesov, B. A. et. al. "Native of the ~1.2 eV Luminescence Band of Gallium Arsenide," Soviet Physics Semiconductors, 8: 425-427 (October, 1974).
34. Bois, D. et. al. "Optical Properties of the Oxygen Center in GaAs," Institute of Physics Conference Series, No. 43: 295-298 (1979).
35. Domanevskii, D. S. and V. D. Tkachev. "Impurity Cathodoluminescence of Semi-insulating Gallium Arsenide," Soviet Physics - Semiconductors, 4: 1790-1793 (May, 1971).
36. Ruo-Zhuang, L. and Wen-Lin, F. "LCAO-MO Treatment of Deep Levels Produced by Ion Implantation of Oxygen in Gallium Arsenide," International Journal of Quantum Chemistry, 18: 601-605 (1980).

37. Henisch, H. K. Rectifying Semiconductor Contacts.  
Oxford: The Clarendon Press, 1957.
38. van der Pauw, L. J. "A Method of Measuring Specific Resistivity and Hall Effect of Discs of Arbitrary Shape." Phillips Research Reports, 13: 1-9 (1958).
39. Baron, R. et. al. Electrical Behavior of Group III and V Implanted Dopants in Silicon." Journal of Applied Physics, 40: 3702-3719.
40. Carter, G. and Grant, W. A. Ion Implantation of Semiconductors. London: Arnold Hall Publishers Ltd.
41. Chandra, A. et.al. "Surface and Interface Depletion Corrections to Free Carrier Density Determinations by Hall Measurements," Solid State Electronics, 12: 645 (1979).
42. Jam, J. F. and R. S. Stermberg, The Design of Optical Spectrometers. London: Butler an Tanner LTD, 1969.
43. Ashen, D. J. et. al. "The Incorporation and Characterization of Acceptors in GaAs", Journal of Physics Chemicals and Solids, 36: 1041-1053 (1975).
44. Kunzel, H. and K. Ploog. "The Effect of As<sub>2</sub> and As<sub>4</sub> Molecular Beam Species on Photoluminescence of Molecular Beam Epitaxially Grown GaAs," Applied Physics Letters, 37: 416-418 (15 August 1980).
45. Mendez, E. E. et. al. "Photoluminescence Study of the Incorporation of Silicon in GaAs Grown by Molecular Beam Epitaxy," Journal of Applied Physics, 54: 4202-4204 (July, 1983).
46. Sydenstricker, R. M. Unpublished Dissertation, AFIT, WPAFB OH: "Electrical, Luminescence and Sims Characterization of Carbon Implanted Vapor Phase Epitaxial Gallium Arsenide," December 1983.
47. Tajima, M. "Deep Level Photoluminescence Commonly Present in Undoped Czochralski Grown GaAs," Applied Physics Letters, 46: 484-486 (1 March 1985).

## Vita

Kevin J. Keefer was born 19 August 1959 in Fort Wayne, Indiana. He graduated in 1977 from Lyons Township High School in LaGrange, Illinois, and subsequently entered the United States Air Force Academy. He graduated in 1981 with a Bachelor of Science degree in Atmospheric Physics. He then pursued graduate studies in Systems Management at the University of Southern California in Los Angeles, California, and attained a Master of Science degree in 1983. His Air Force career has included an assignment as a project officer at the Ballistic Missile Office, Norton Air Force Base, California (1981-1984). In 1984 he entered the Air Force Institute of Technology at Wright-Patterson Air Force Base, Ohio, to pursue a Master of Science degree in Engineering Physics.

Permanent Address: 5112 Wolf Rd.  
Western Springs, Illinois

UNCLASSIFIED

SECURITY CLASSIFICATION OF THIS PAGE

## REPORT DOCUMENTATION PAGE

1. REPORT SECURITY CLASSIFICATION <b>UNCLASSIFIED</b>		1b. RESTRICTIVE MARKINGS <b>NONE</b>							
2a. SECURITY CLASSIFICATION AUTHORITY		3. DISTRIBUTION/AVAILABILITY OF REPORT Approved for public release; distribution unlimited.							
2b. DECLASSIFICATION/DOWNGRADING SCHEDULE									
4. PERFORMING ORGANIZATION REPORT NUMBER(S) <b>AFIT/GEP/85D-8</b>		5. MONITORING ORGANIZATION REPORT NUMBER(S)							
6a. NAME OF PERFORMING ORGANIZATION School of Engineering Air Force Inst. of Tech.	6b. OFFICE SYMBOL (If applicable) <b>AFIT/EN</b>	7a. NAME OF MONITORING ORGANIZATION							
6c. ADDRESS (City, State and ZIP Code) <b>Wright-Patterson AFB, OH 45433</b>		7b. ADDRESS (City, State and ZIP Code)							
8a. NAME OF FUNDING/SPONSORING ORGANIZATION	8b. OFFICE SYMBOL (If applicable)	9. PROCUREMENT INSTRUMENT IDENTIFICATION NUMBER							
8c. ADDRESS (City, State and ZIP Code)		10. SOURCE OF FUNDING NOS. <table border="1"><tr><td>PROGRAM ELEMENT NO.</td><td>PROJECT NO.</td><td>TASK NO.</td><td>WORK UNIT NO.</td></tr></table>		PROGRAM ELEMENT NO.	PROJECT NO.	TASK NO.	WORK UNIT NO.		
PROGRAM ELEMENT NO.	PROJECT NO.	TASK NO.	WORK UNIT NO.						
11. TITLE (Include Security Classification) <b>See Box 19</b>									
12. PERSONAL AUTHOR(S) <b>Kevin J. Keefer, Capt, USAF</b>									
13a. TYPE OF REPORT <b>MS Thesis</b>	13b. TIME COVERED FROM _____ TO _____	14. DATE OF REPORT (Yr., Mo., Day) <b>85 Dec</b>	15. PAGE COUNT <b>90</b>						
16. SUPPLEMENTARY NOTATION									
17. COSATI CODES <table border="1"><tr><td>FIELD</td><td>GROUP</td><td>SUB. GR.</td></tr><tr><td><b>20</b></td><td><b>12</b></td><td></td></tr></table>		FIELD	GROUP	SUB. GR.	<b>20</b>	<b>12</b>		18. SUBJECT TERMS (Continue on reverse if necessary and identify by block number) <b>Silicon and Oxygen Implanted Gallium Arsenide, Photoluminescence, Ion Implantation, Gallium Arsenide</b>	
FIELD	GROUP	SUB. GR.							
<b>20</b>	<b>12</b>								
19. ABSTRACT (Continue on reverse if necessary and identify by block number)  Title: <b>PHOTOLUMINESCENCE STUDY OF SILICON AND OXYGEN IMPLANTED GALLIUM ARSENIDE</b>  Thesis Advisors: <b>Dr. R.L. Hengehold; Dr. Y.K. Yeo</b>  <div style="text-align: right;"><i>Approved for public release LAW 278 2004</i> <b>LARRY E. WOLAYER</b> <b>13 Feb 86</b> Dean for Research and Professional Development Air Force Institute of Technology (AFIT) Wright-Patterson AFB OH 45433</div>									
20. DISTRIBUTION/AVAILABILITY OF ABSTRACT <b>UNCLASSIFIED/UNLIMITED <input checked="" type="checkbox"/> SAME AS RPT. <input type="checkbox"/> DTIC USERS <input type="checkbox"/></b>		21. ABSTRACT SECURITY CLASSIFICATION <b>Unclassified</b>							
22a. NAME OF RESPONSIBLE INDIVIDUAL <b>Dr. R.L. Hengehold; Dr. Y.K. Yeo</b>		22b. TELEPHONE NUMBER (Include Area Code) <b>513-255-2012</b>	22c. OFFICE SYMBOL <b>AFIT/ENP</b>						

The low temperature photoluminescence properties of Si-, 0- or (Si+0)- implanted GaAs have been analyzed. Liquid Encapsulated Czochralski (LEC) grown GaAs was implanted with 100 keV silicon ions at a dose of  $6 \times 10^{12} \text{ cm}^{-2}$  and/or 65 keV oxygen ions at a dose of  $1.5 \times 10^{12}$  or  $3 \times 10^{12} \text{ cm}^{-2}$ . The oxygen ion energy was chosen so that its projected range coincided with that of the silicon ion. The Si-implanted layers were annealed at 850°C for 15 minutes. The 0- and (Si+0)- implanted samples were annealed at 400°C for two hours or 900°C for 15 minutes.

Electrical measurements indicated that GaAs:Si+0 layers annealed at 400°C had resistivities four orders of magnitude larger than the Si-implanted layers. In contrast, the resistivity of the GaAs:Si+0 layers had increased by only a factor of one and a half when annealed at 900°C.

By comparing spectral features of the differently prepared samples as a function of sample temperature as well as depth within the sample, it was found that there was some correlation between the electrical and optical properties of these layers. The free-to-bound transition ( $e, \text{Si}_{\text{As}}$ ) in the GaAs:Si layers was quenched in the 400°C annealed GaAs:Si+0 layers, which in turn exhibited relatively high resistivity. However, this particular transition was found in the relatively low resistivity GaAs:Si+0 layers annealed at 900°C. It is proposed that the implanted oxygen created intermediate levels in the high resistivity samples. The formation of these levels in the low resistivity samples was inhibited, as oxygen appeared to assist rather in the creation of Q-band related complexes that had been normally found in GaAs:Si layers which were capped and annealed.

END  
FILMED

5-86

DTIC